Wind turbine tower collapse due to flange failure: FEM and DOE analyses

Mar Alonso-Martinez [a*], José M. Adam[b], Felipe P. Alvarez-Rabanal[a],

Juan J. del Coz Díaz[a]

[a]*Department of Construction, EPSIII, University of Oviedo, 33204 Gijón, Spain*

[b]*ICITECH, Universitat Politècnica de València, Camino de Vera s/n, 46022 Valencia, Spain*

ABSTRACT

Although a large number of papers have been published to date on failures in wind turbines, most of them have focused on blade failures and less attention has been paid to the tower failures. This paper analyses the causes that led to the failure of one element that finally caused the whole tower to collapse. A diagnosis of the cause of the failure was carried out after an initial on-site inspection, when the origin of the failure appeared to be in the flange that joined the tower to its base. An experimental program was carried out to analyze the characteristics of the steel in the area nearest to the flange. A non-linear simulation was then performed by the finite element method (FEM) of the flange area where the failure had occurred, including the bolts, their prestressing forces and the contact between the joined surfaces. In order to study the influence of different variables on the flange's structural response, a method based on the Design of Experiments (DOE) was used on the FEM model. Finally, the main lessons learnt from the experience are given with the aim of contributing to improving the design and construction of wind turbine towers.

Keywords: Wind tower; Collapse; Failure; Design of experiments; Finite element modeling

* Corresponding author: Mar Alonso-Martinez

E-mail address: mar@constru.uniovi.es

Postal address: EDO 7. Room 7.1.28.

Campus de Viesques. Gijon. Asturias

CP: 33204. Spain

1. Introduction

The development of alternative sources of energy to fossil fuels has made steady progress since the world energy crisis of the seventies and has expanded with the search for clean forms of renewable energy, of which wind power has played an important role, due to its technology, infrastructure and relatively low cost [1].

Wind power is produced by using the action of the wind on an electric generator known as a wind turbine, whose main parts are the rotor blades moved by the wind, joined to an electric generator incorporating specific system management components for generating and transmitting electricity. All the equipment is supported by a tower held in place on its foundations.

In order to increase the efficiency of wind turbines, the size of these towers has continually grown throughout the years [1, 2]. The 2-3 MW wind turbines that used to dominate the market have been replaced by those of 3-5 MW [1].

At the present time most of the towers are constructed of steel tubes. The first models were built with steel lattices, but as they grew in size this system was considered inappropriate and they were replaced by the steel tubes now in use. These tower tubes are usually manufactured in two or three segments that are joined together on site, either by bolts and flanges or by welding.

The ever-increasing size of the wind turbines have meant that static calculation methods, which assumed a constant wind speed, have been replaced by dynamic simulation software that allows the aero-elastic response of the complete wind turbine to be simulated with variable dynamic loads, including the tower, the drivetrain, the rotor blades and the control system [1].

The complexity of the wind turbine structures and its components has also been the cause of a number of serious accidents. These wind turbines are generally, though not always; in the form of wind farms situated in open spaces far from residential areas. When they are close to infrastructures and built-up areas they may be a serious risk.

Wind turbine failure is often due to the failure of rotor blades or of the steel tower [3, 4]. Many papers have been published on blade failures containing simulation by numerical methods or experimental tests [4–11]. When the tower collapses it can cause serious damage to property entailing financial losses and may be due to diverse causes, one of which is the buckling of the steel tower, as pointed out in Lee & Bang [12]. Other possible causes include steel fatigue due to vibration or being shaken by the wind, failure or incorrect placement of the bolts in the base of the structure or in the joints between the different steel tube sections, as described in Chou & Tu [13].

The investigation and study of real failures can provide important information for the improvement of the design of structural elements based on new theories, concepts, construction details, monitoring, etc. [14-16]. The reason for publishing the present study was because only a few papers have been published on the particular case of wind turbine towers. The paper is organized as follows: firstly, the main characteristics of a wind turbine are given, followed by the description of the collapse of one of these structures due to the failure of the tower. The causes of the failure were determined by: visual inspection, laboratory tests, a Finite Element Method (FEM) simulation of the zone in which the failure occurred, and a Design of Experiments (DOE) to assess the influence of the different parameters involved in the

71　risk of structural collapse. In the final section, the lessons learnt from the study are given with the aim

72　of contributing to improving the design and construction of wind turbine towers.

73

2. Description of the wind turbine

75　The *Abuela de Santa Ana* onshore wind farm is located near the town of Pozo Llorente in the province

76　of Albacete (Spain). It consists of 25 GE Energy 1.5sle Model 1.5KW wind turbines, the diameter of

77　the rotor is 77m and the height of the tower varies between 61.4m and 85m. It is operational at the

78　present time under the control of the ACS Company at a nominal power of 37.500 kW. Its geographic

79　coordinates are 39° 4' 36.5" latitude and -1° 30' 23.5" longitude. A view of the wind farm with a close-up

80　of a tower can be seen in Fig. 1.

81　　　　　　*Fig. 1.　　　General view of the Abuela de Santa Ana wind farm and one of the towers*

82　The turbine towers are composed of different steel tubes and the flange is fixed to the lower tube and is

83　embedded in the foundations (see Fig.2). The tower tubes are bolted together and are required to

84　maintain the necessary stiffness to support the turbine nacelles fixed to the top of the tower.

85　The flange is placed in the lower part of the tower. The flange is a steel tube 1.67 m long and 4.3 m

86　diameter. It consists of the following components (see Fig. 2):

87　　-　Lower T-flange to transmit loads to the foundations.

88　　-　Upper flange fixed to the next tower section by M36a bolts.

89　　　　　*Fig. 2.　　　Details of the tower/foundation connection.　a) Detail of lower flange and foundation;*

90　　　　　　　　　　　　　　　*b) Detail of flange and bolts. Source: [17]*

91　The lower tube is totally embedded in concrete except for the upper 0.2 m which are available for

92　bolting to the tower shell. Due to its failure, the flange in one of the towers between the foundations

93　and the structure was the object of the present study.

94

3. Collapse of the turbine tower

96　In October 2008, two months after being out into operation, one of the *Abuela de Santa Ana* wind

97　turbine towers collapsed due to a catastrophic failure in the lower flange fixed to the foundations. An

98　on-site inspection of the damage was made the following day.

99　Firstly, the joint between the tower and the nacelle was seen to be in good condition with no evidence

100　of damage at this location having caused the failure. Secondly, the steel tube was buckled, as can be

101　seen in Fig. 3. Thirdly, the blades were seen to have damaged the steel tubes during the fall. After the

102　inspection, the most probable cause was therefore identified as the failure of the base of the tower,

103　which was made the focus of future tests to find the definite cause of the collapse.

104　　　　　　　　　　　*Fig. 3.　　　View of the tower the day after collapsing*

105　After the base had been analyzed in greater detail, the failure was located in the lower flange. This

106　component had been built from a bar of rectangular cross-section, curved and welded S-355-J2 steel

107 according to the UNE-EN-10025-3:2006 code [18] and in the zone of the failure had been welded to a
108 steel tube.

109   *Fig. 4.   View of the section in which the failure began*

110 The damaged zone (See Fig.4) showed signs of corrosion, which would later be analyzed to identify
111 the type of failure and its causes. This section was covered with a plastic sheet in order to keep these
112 zones intact and avoid any deterioration in the material due to the weather subsequent to the collapse
113 that could possibly lead to errors in the conclusions of the analysis.

114 The preliminary visual study identified a sector of approximately 3 m. that had been badly affected by
115 black, blue and brown colored oxidation, in contrast to the rest of the section in which the surface was
116 seen to be clean (Fig.4).

117

118 **4. Analysis of the collapse**

119 *4.1. Visual inspection of the broken section*

120 A scheme of the flange studied in this work can be seen in Fig. 5. The flange had been positioned in
121 order of the drill holes numbered from 1 to 138, number 1 being at the centre of the lower tower access
122 door. The broken section to be studied in detail was joined to the flange whose scheme is shown in Fig.
123 5.

124   *Fig. 5.   Detail of the flange and position of the cracks*

125 The broken section was found to have started and propagated in the base of the flange neck (see Fig.6a).
126 In photographs taken days after the collapse, various cracks were located in the flange cross-section, as
127 can be seen in Fig. 6:

128   -   The initial crack was located between drill holes 100 and 130 (see Fig.6c)
129   -   Between drill holes 109 and 123 black and blue rust stains were observed (see Fig.6b). These
130   stains were visible in the on-site inspection and were thus assumed to exist before the collapse
131   of the structure.

132 In view of the above, the start of the break was considered to date approximately from the time when
133 the tower had been constructed, due to the oxidation in the broken section.

134 The failure mode observed in the flange provided information to make a preliminary diagnosis of the
135 collapse that would later be verified by experimental tests and numerical analysis. This diagnosis
136 identified the initial crack that did not spread any further and that could have been due to the forces
137 induced by the bolt pretension or also possibly by a crack in the flange due to an impact during its
138 installation in the tower.

139   *Fig. 6.   Detail of the damaged flange section. a) Side view; b) Top view; c) Detail of crack*
140   *start point*

141 The detailed analysis of the oxides found in the damaged section included a large amount of blue oxides
142 organized into bands or groups of points (see Fig. 6c and Fig. 7) characteristic of the so-called *blue*

143 *brittleness* or *brittle martensite.* The former is often found in most steels and is due to the transformation
144 of austenite into cementite at the grain boundaries when the material is subjected to temperatures around
145 300º C. The decomposition of the austenite seriously reduces the toughness of the material. This type
146 of brittleness is accentuated by the segregation of impurities at the grain boundary, which promotes the
147 intergranular breaks typical of brittle fractures [19] and [20]. Some authors have observed that blue
148 brittleness when combined with corrosion cracks can cause disastrous failures in steel components [21–
149 23].

150 *Fig. 7.   Detail of the broken flange section*

151 From the initial analysis based on measurements taken on site and a visual inspection, it was considered
152 that the failed flange could have been the determining factor in the collapse of the tower. Details of the
153 flange manufacturing process are given in the following section.

154

4.2. Flange manufacturing process

156 The flange dimensions are as follows: 4.3 m. external diameter, 0.107 m. maximum thickness, and 0.15
157 m. in width, with 138 drill holes of 0.039 m. in diameter. The section geometry and tolerances are given
158 in Fig. 8.

159 *Fig. 8.   Geometry of flange section*

160 The flange was made from a rectangular section S-355-J2 steel bar (dimensions: 4.3x0.17x0.12
161 mxmxm) according to UNE-EN 10025-3:2006 [18]. The first treatment is the normalizing, after which
162 it is cold formed and welded. The next step is the thermal treatment to eliminate any residual stresses
163 after cold-forming. In the final stage it is machined into the required shape within the necessary
164 tolerances. Mechanical properties of this material are well known. Quality tests were done by the steel
165 manufacturer to ensure the material properties of the project requirements.

166

5. Experimental tests

168 In view of the type of failure discovered in the flange, close to the welded zone, the material was
169 analyzed to obtain the fracture toughness parameters. Three Charpy specimens were extracted from the
170 flange between drill holes 112 and 114, as shown in Fig. 9 [24].

171 *Fig. 9.   Detail of the specimen extraction zone. Source [24]*

172 The tests gave mean toughness values of 13 Joules for specimen W (working direction), i.e. in the
173 direction of the tower generatrix (direction of tensile stresses in the flange when the structure is
174 subjected to bending forces), and 10 joules for specimen M (manufacturing direction), i.e. longitudinal
175 direction of laminated bar from which the flange is formed, as shown in Table 1.

176

177 Table 1.   Experimental Results

	Sy (MPa)	Su (MPa)	A (%)	Kv (+13ºC) (J)	Kv (-20ºC) (J)
Flange W (*)	422	557	24	62	13
Flange M (**)	383	536	28	---	10
S355 J2	>295	450-600	>18	---	>27

(*) W: Working direction

(**) M: Manufacturing direction

Reference values obtained for S355J2 grade with 105 mm width from UNE-EN 10025-2 [25].

Yield strength (Sy), Tensile Strenght (Su), Deformation (A), Toughness (Kv)

178

179 Since the value was below the 27 J given in the EN10025-3 Code [18], it was therefore concluded that
180 the fracture toughness of the material was unsatisfactory in all directions. In view of these results, a
181 serious weakness was identified in the material that could have been responsible for unforeseeable
182 failures in the behavior of the structure. The experimental results show that the material does not possess
183 the properties required by the current code and this anomaly could have caused the abnormal behavior
184 of the structure that had not been considered in its design.

185

186 **6. Finite element modelling**

187 In the present work, a numerical model based on Finite Element Method studied the behavior of the
188 flange in order to analyze the cause of the collapse. The procedure followed in this stage consisting of
189 a detailed geometrical model of a sector of the flange, taking advantage of its symmetry. The upper and
190 lower steel tubes were included, as were the zones affected by welding and the bolts.

191 FEM makes it possible to calculate strains and stresses and the possible failure modes under a range of
192 stresses and working conditions [26]. Ansys-Workbench R16.1 Academic software [27] and [28] was
193 used for this study.

194 The analyses were supplemented by a design of experiments (DOE) study (see Section 7) in which the
195 influence of the different input variables was assessed to identify the response of the flange under
196 different conditions.

197

198 *6.1. Material properties and geometry*

199 The materials were modelled considering the steel's elastic properties with linear behavior until
200 yielding. The defined material was steel with a modulus of elasticity of 200 GPa and a Poisson's
201 Coefficient of 0.3, yield strength of 250 MPa and ultimate tensile strength of 460 MPa. These properties
202 have been taken from the manufacturer datasheet.

203 The geometrical model studied consisted of the lower flange, the upper flange and a bolt joining both
204 parts, to which symmetry conditions were applied in order to reduce the computational cost of the
205 models. Details of the model geometry can be seen in Fig. 10.

206 *Fig. 10.   Geometric model: a) Lower flange; b) Upper flange and bolt; c) Complete*
207 *(symmetry) model.*

208

6.2. Finite elements used and contact model

210 SOLID95 type finite elements were used for the flange and SHELL93 for the steel tube at a distance
211 from the joint (see Fig.11a). These elements are suitable for modelling curved zones and complex
212 geometries, as in the case under study [25–27].

213 SOLID95 is a 3-D element with 20 nodes and three degrees of freedom able to accurately simulate
214 irregular geometries and structural phenomena such as plasticity, creep and large deformations, among
215 others [29].

216 SHELL93 is an element defined by 8 nodes and three degrees of freedom in each node (displacement
217 and rotations in three directions of the space) and is suitable for curved plate models such as the steel
218 tube at a distance from the joint in the present study [29].

219 The mesh size was minimum 0.0013 m and maximum 0.27 m, with a total of 266.194 nodes and 71.117
220 elements. As can be seen in Figure 11b, certain zones of the geometry were modelled with a very fine
221 finite elements mesh due to the curves and transitions between the elements.

222 *Fig. 11.   Finite elements mesh: a) General view; b) Detail of the mesh in the bolt*
223 In this case, the average element quality ratio is 0.806 out of 1. In consequence, numerical results are
224 in good agreement with the expected behavior. For three-dimensional elements, this metric is based on
225 the ratio of the volume to the sum of the square root of the sum of the square of the edge lengths.

226 The model was completed with the configuration of the contact between elements and the application
227 of boundary conditions, which consisted of frictional contact between the flanges surfaces and bonded
228 contact between the bolt head and the upper flange surfaces and for the nut with the lower flange
229 surfaces (see Fig.12). The friction coefficient considered was 0.1, adopting an Augmented Lagrangian
230 formulation [30].

231 *Fig. 12.   Contacts in model*

232

6.3. Loads and boundary conditions

234 This section provides details of the loads applied to the finite element (FE) model and the boundary
235 conditions considered for the joint as well as the simplification procedure in order to obtain realistic
236 values and structural response from the engineering point of view.

237 To begin with, use was made of the flange symmetry to simplify the model and represent the actual
238 continuity of the tower shell and flanges. In this way, only a 1/138th sector of the flange was simulated
239 and symmetry conditions were applied (see Fig. 13). Secondly, a restriction was applied on the

240   displacements at the lower end of the foundation steel tube (A in Fig. 13). Thirdly, a load was applied
241   on the upper end of the joint (B in Fig. 13) representing the vertical load exerted on the foundation by
242   the structure and its various components. Additionally, other loads present in the structure were applied,
243   whose values were provided by the manufacturer of the tower (C and D in Fig. 13). The loads applied
244   on the model and their values (see Fig. 13) were as follows:

245   -   Fixed support on the base of the foundation steel tube (A in Fig. 13).
246   -   Compression load on the upper steel tube of the flange to the value of 32.57 kN (B in Fig. 13).
247   -   Load applied on all the steel tube in a direction perpendicular to the axis of the tower
248   corresponding to the maximum wind pressure on the structure, whose value is $1,236 \cdot 10^{-3}$ MPa
249   (C in Fig. 13).
250   -   A pretension load applied on the bolt joining the upper and lower flanges at a value of 519.91kN
251   (D in Fig. 13).

252   The force generated by the wind on the blades causes a bending moment at the base of the tower that
253   subjects the joint to tensile and compressive forces. There are several ways to obtain the wind load on
254   the blades [13], [10]. The use of Computer Fluid Dynamics (CFD) is a useful methodology to obtain
255   the wind load on blades including the aeroelastic behavior. Other authors used this methodology in the
256   last years [31]. Furthermore, the influence of the blade material properties on the tower wind load could
257   be taking into account [32]

258   In the present work, the load is obtained following the standards and guides as follows [33]. This
259   horizontal force is limited by the available power, P_a. The available power is obtained by applying a
260   correcting ratio to the power generated due to the kinetic energy of the wind, P (see Eq. (1)). The
261   maximum efficient power of a turbine is restricted by the Betz Limit, which is called the "power
262   coefficient", C_p [33]. Betz's Law defines this coefficient for any design of wind turbine at 0.59. Despite
263   the fact that Betz Law establishes the theoretical maximum power efficiency at 59%, other factors such
264   as strength or durability reduce this value to 0.35 – 0.45. Usually, for high performance equipment, the
265   Betz limit value considered is 0.4.

266   $P_a = C_p \cdot P$ Eq. (1)

267   The power generated is determined by the kinetic energy of the wind in accordance with Eq. (2).

268   $P = \frac{1}{2} \cdot \rho \cdot A \cdot v^3$ Eq. (2)

269   Where:

270   ρ: Air density in kg/m^3

271   A: Area swept by rotor in m^2

272   v: Linear velocity of the wind in m/s

273   The horizontal force on the rotor is determined by Eq. (3).

274   $F = \frac{P_a}{v} = \frac{C_p \cdot P_d}{v}$ Eq. (3)

275   Data on the characteristics of the rotor are required for calculating the horizontal force. The
276   characteristics are specified in Table 2.

277

278   Table 2.   Wind turbine information

Wind power component	Values
Rotor diameter, D (m)	77
Swept area, A (m²)	4 656.6
Nacelle weight, (kg)	50 000
Rotor + hub weight (kg)	31 000
Wind Speed, v (m/s)	5.21

279

280   The values obtained for the power and for the horizontal force on the rotor are shown in Table 3.

281

282   Table 3.   Power and load on the wind turbine.

Loads	Values
Power (kW)	742.41
Avaliable Power (kW)	296.96
Wind force (kN)	46.57

283

284   The maximum tensile stress on the tower flange is due to two main forces (see Eq. (4)):

285   -   The bending moment caused by the horizontal force of the wind on the rotor.
286   -   The weight of the turbine unit and the tower, which generate a normal force on the flange.

287    $\sigma_{\max (c)} = \dfrac{M_f}{W_f} + \dfrac{P_p}{S}$ Eq. (4)

288   Where:

289   M_f: Bending moment on the tower flange (kN·m)

290   W_f: Bending resistance (m³)

291   P_p: Self-weight (kN)

292   S: Cross-section area of the tower (m²)

293   The bending moment in the tower flange is obtained by multiplying the horizontal force on the rotor by
294   the distance to the base of the tower (Eq. (5)).

295    $M_f = F \cdot d \cdot \gamma$ Eq. (5)

296   Where:

297   F: Horizontal force generated by the wind (kN)

298   d: Distance to the base of the tower, 80 m.

299   γ: Safety factor, 1.5

300   To calculate the self-weight, the weight of the tower ($P_{w\text{-}tower}$) and the weight of the turbine unit ($P_{w\text{-}turbine}$) comprising the nacelle, rotor and hub must all be taken into consideration (Eq. (6)). Data
301
302 necessary to obtain $P_{w\text{-}tower}$ and $P_{w\text{-}turbine}$ are shown in Table 2.

303     $P_p = P_{w-tower} + P_{w-turbine}$ Eq. (6)

304   The weight of the tower ($P_{w\text{-}tower}$) is 169.67 kN, and the weight of the wind turbine ($P_{w\text{-}turbine}$) is 810 kN,
305 including the nacelle, rotor and hub[34]. Therefore, the self-weight of the wind turbine (P_p) is 979.67
306 kN.

307   By using these data, the maximum stress on the flange can be expressed by Eq. (4), while the minimum
308 stress can be determined by the tensile stress on the flange (Eq. (7)).

309     $\sigma_{\min\,(t)} = \dfrac{M}{W_f} - \dfrac{P_p}{S}$ Eq. (7)

310   The stress values on the flange are shown in Table 4.

311   Table 4.   Stress values on the flange

Stress	
Max. Compression Stress $\sigma_{\max\,(c)}$ (MPa)	16.64
Max. Tensile Stress $\sigma_{\max\,(t)}$ (MPa)	9.38
Max. Compressive load (kN)	(-)32.57
Tensile Load (kN)	(+)18.37

312

313   Based on the results obtained, the normal load applied to the flange was varied between 15 kN of
314 maximum tensile load and 40 kN of maximum compressive load for the study of all the states of
315 intermediate loads between the maximum load (compressive) and the minimum load (tensile).

316   *Fig. 13.   Boundary conditions used on a section of the flange*

317 The computational calculation was performed by means of the Newton-Raphson iterative method,
318 based firstly on the pretension analysis of the bolt with a subsequent application of all the loads required
319 by the flange. The pretension load is modelled using a set of pretension elements (element type
320 PRETS179), [28]. This element has one translation degree of freedom, which is the pretension direction.
321 The surfaces connected by the pretension elements must be matched using coincident nodes in both
322 meshes to obtain accurate results. A total of 8 sub-steps and 17 iterations were necessary before model
323 convergence was achieved.

6.4. Analysis of the results

The results obtained from the numerical simulations provided interesting information for an exhaustive analysis of the tower failure. On analyzing the stresses in the joint it was seen that the prestressing of the bolts, before considering the other loads, exerts high forces on the joint, as can be seen in Fig. 14a, since the flange steel's yield strength is exceeded. As a result, the flange is already in a highly stressed state even before the other loads on the structure are taken into account.

After applying loads on the structure, the numerical model showed a high concentration of stresses on the flange neck that coincided with the point of the failure observed in the visual inspection. After analyzing the results of the numerical model, it is shown that the Maximum Von-Mises stress exceeded the material's yield strength (see Fig.14b).

Fig. 14 gives the most important results of the Von Mises stress distribution in the flange. Fig. 14a shows the stress state of the joint when subjected to bolt pretension only. Fig. 14b includes the stress state of the flange when subjected to all the loads.

Fig. 14.   FEM model results, equivalent Von-Mises stress. a) applying bolt pretension only (in MPa); b) for all applied loads (in MPa)

7. Design of experiments (DOE)

7.1. General information

Design of Experiments (DOE) is a technique used to identify the influence of input parameters on output parameters, as well as to optimize the analysis results. This technique is widely used in engineering to obtain results from a range of input parameters using a minimum of input sampling points. Response surface provide intermediate results. The accuracy of the response surface depends on the type of DOE and the number of cases studied, [35].

In this work, a DOE, type Central Composite Design (CCD), was used to study the influence of certain conditions on the level of stresses in each part of the flange section. This method was used by the authors in previous work on the analysis of structural failures and to optimize new designs [32–34].

In this case, the focus was on the flange bolt pretension, the coefficient of friction in the flange contact, and the vertical force on the flange, which could affect the structural integrity of the joint. The output parameters studied were the maximum stress on the[35] joint and the maximum Von Mises stress in the analysis. Table 5 gives the maximum values adopted for the input variables and their initial values.

Table 5.   Values of parameters in the DOE

	Minimum Value	Initial Value	Maximum Value
Frictional Coefficient	0.1	0.1	0.3
Bolt preload (kN)	100	520	571
Force (Y axis) (kN)	-40	32.5	15

358 The analysis identified the individual critical stress values for each element under different load states.
359 The results obtained allowed us to identify the most important critical points in the joint, the influence
360 of the input variables on each one, and the permitted load limits to keep the structure in a state of stress
361 within the material's admissible limits.

362 The DOE analysis can identify the cause of the fracture of the joint, the load limits that would cause the
363 collapse of the structure and the different load combinations that would overload the joint and cause it
364 to have brittle behavior.

365

366 ## 7.2. Analysis of the results

367 The maximum stress values were the most important results obtained from the numerical analysis of
368 the joint, including the contact stress between both flanges and the individual stress level of both the
369 upper and lower flanges.

370 In regard to the flange contact pressure (see Fig.15a), the maximum value obtained was in the central
371 axis of the surface and reached a value of 62.8 MPa. The maximum Von Mises stress values in upper
372 and lower flanges were very high (see Figs. 15b and 15c).

373 *Fig. 15.   Results of the FE model and DOE analysis: a) Contact stress between upper and*
374 *lower flanges (in Pa); b) Von Mises stress in upper flange (in Pa); c) Von Mises stress in*
375 *lower flange (in Pa)*

376 The DOE results also contributed to the diagnosis of the collapse of the structure by identifying the the
377 most influential variables of the limit stress state of the joint. In the sensitivity analysis shown in Fig.
378 16, it can be seen that the most influential parameter is the pretension stress applied to the bolt, followed
379 by the vertical component of the load applied to the steel tube, and lastly the coefficient of friction
380 between the contact surfaces of the flanges.

381 *Fig. 16.   Sensitivity analysis*

382 Fig. 17 shows the response surface that reflects the variation in maximum Von Mises stress in the
383 different parts of the upper and lower flanges. In both cases the maximum Von Mises stress considered
384 was in the part nearest to the steel tube, since, as was seen previously, this is the zone of the flange with
385 the highest concentration of stresses.

386 The response surfaces obtained from the DOE had maximum values very similar to the upper and lower
387 parts of the flange. It was also seen that the bolt pretension load had a greater influence than the vertical
388 load on the steel tube in the maximum von Mises stress value.

389 *Fig. 17.   DOE analysis: External part of the flange (upper and lower part. a) Bolt pretension*
390 *vs Force Y in upper part of the flange; b) Bolt pretension vs Force Y in lower part of the*
391 *flange*

392 Fig. 18a shows the influence of the bolt pretension load and of the coefficient of friction with respect
393 to the pressure in the contact between the flanges. It can be seen that the most influential parameter is
394 the pretension load. Figure 18b shows the influence of the vertical load on the pressure value; it can be
395 seen that the greatest influence is due to the vertical load applied to the steel tube.

396 *Fig. 18.   DOE analysis: maximum pressure in contact between the flanges: a) Contact friction*
397 *vs Bolt pretension; b) Contact friction vs Force Y.*

399

8. Diagnosis

401 In the visual inspection carried out on site it was determined that the failure had occurred in two phases
402 in a brief interval of time:

1) The initial failure appeared to be caused by force that disappeared after the crack started (a case of imposed deformation and/or a temporary force derived from an undue event). After this study, it was considered that the failure occurred during the building of the turbine tower, when the pretension was applied to the bolts.
2) The second failure occurred when the tower was in service and the resistant section became weakened because of the initial fracture and progressed until the tower collapsed.

410 The presence of blue oxides in the fracture zone indicated the possibility of a defect in the manufacture
411 of the element. To verify this, experimental tests were carried out on the toughness of the steel used in
412 the tower and showed that the steel did not meet the requirements of the resilience test. The steel was
413 shown to have very low toughness and was not suitable for use in the structure.

414 FEM numerical simulations and DOE were used in the present study to analyze the collapse of the wind
415 turbine tower. The results obtained showed that the pretension of the bolts, before considering the
416 remaining forces, exerted considerable stresses on the joint (Fig.14a) that reached the yield strength of
417 the steel in the flange. This high concentration of stresses occurred precisely at the fracture point in the
418 flange neck observed in the visual inspection. The sensitivity analysis by DOE (Fig.16) also showed
419 that the most influential parameter in regard to the von Mises stresses in the joint was the preload stress
420 applied to the bolts. Finally, the response surfaces obtained from the DOE analysis showed that the bolt
421 pretension load had a clearly greater influence than the vertical load and the coefficient of friction in
422 the value of the maximum von Mises stress throughout the range of loads applied to the flange.

423 Therefore, based on the visual inspection, the laboratory tests carried out and the numerical technique
424 employed (FEM models, sensitivity analysis, response surfaces and the DOE-based method) it can be
425 stated that the collapse of the tower was due to defective material combined with errors in the design of
426 the flange. Both issues make the stress due to the bolt pretension combined with the residual welding
427 stresses are higher than the strength and toughness of the flange material.

428

9. Conclusions and lessons learned

430 This paper analyze the collapse of a wind turbine tower. The causes of the failure were determined by
431 a visual inspection, laboratory tests, FEM simulations and a subsequent DOE analysis. The main lessons
432 learned can be summed up as follows:

1. On-site inspection of the collapsed structure is essential, together with the immediate isolation of the fractured section to avoid any changes due to oxidation or other agencies.
2. The observation of the fractured section and detailed photographs of all sectors to show differences in colour or appearance can also contribute to clarifying the causes of a collapse.

3. The experimental analysis of all material properties such as resistance or toughness is fundamental to establish the possible causes of the failure.
4. The creation of detailed FEM models to study the load distribution in the broken section enable the analysis of possible causes of the failure.
5. Applying the DOE technique in the study provides information on the structural behaviour when the physical properties or the loads have wide range of variations and is a fundamental tool for identifying the basic variables involved in the phenomenon.

In the present case, the failure could have been avoided if the material used in the flange had been subjected to the appropriate quality control (toughness test). It could also have been avoided had the flange been better designed to remove the maximum service stress away from the zone affected by the welding, e.g. with a larger chord radius and longer neck.

Acknowledgements

References

[1] C.C. Chia, J.-R. Lee, Hyung-Joon Bang, Structural health monitoring for a wind turbine system: a review of damage detection methods, Meas. Sci. Technol. 19 (2008) 122001. doi:10.1088/0957-0233/19/12/122001.

[2] Y. Lin, L. Tu, H. Liu, W. Li, Fault analysis of wind turbines in China, Renew. Sustain. Energy Rev. 55 (2016) 482–490. doi:10.1016/j.rser.2015.10.149.

[3] Caithness Windfarm Information Forum (CWIF), Summ. Wind Turbine Accid. Data to 30 Sept. 2014. (n.d.). http://www.caithnesswindfarms.co.uk/ (accessed August 9, 2016).

[4] F.P.G. Marquez, J.M.P. Perez, A.P. Marugan, M. Papaelias, Identification of critical components of wind turbines using FTA over the time, Renew. Energy. 87 (2016) 869–883. doi:10.1016/j.renene.2015.09.038.

[5] L.C.T. Overgaard, E. Lund, Structural collapse of a wind turbine blade. Part B: Progressive interlaminar failure models, Compos. Part A Appl. Sci. Manuf. 41 (2010) 271–283. doi:10.1016/j.compositesa.2009.10.012.

[6] M.M. Shokrieh, R. Rafiee, Simulation of fatigue failure in a full composite wind turbine blade, Compos. Struct. 74 (2006) 332–342. doi:10.1016/j.compstruct.2005.04.027.

[7] C. Kong, J. Bang, Y. Sugiyama, Structural investigation of composite wind turbine blade considering various load cases and fatigue life, Energy. 30 (2005) 2101–2114. doi:10.1016/j.energy.2004.08.016.

476 [8] F.M. Jensen, B.G. Falzon, J. Ankersen, H. Stang, Structural testing and numerical simulation of
477 a 34m composite wind turbine blade, Compos. Struct. 76 (2006) 52–61.
478 doi:10.1016/j.compstruct.2006.06.008.

479 [9] L.C.T. Overgaard, E. Lund, O.T. Thomsen, Structural collapse of a wind turbine blade. Part A:
480 Static test and equivalent single layered models, Compos. Part A Appl. Sci. Manuf. 41 (2010)
481 257–270. doi:10.1016/j.compositesa.2009.10.011.

482 [10] C.P. Chen, T.Y. Kam, Failure Analysis of Small Composite Sandwich Turbine Blade Subjected
483 to Extreme Wind Load, Procedia Eng. 14 (2011) 1973–1981. doi:10.1016/j.proeng.2011.07.248.

484 [11] X. Chen, W. Zhao, X.L. Zhao, J.Z. Xu, Preliminary failure investigation of a 52.3m glass/epoxy
485 composite wind turbine blade, Eng. Fail. Anal. 44 (2014) 345–350.
486 doi:10.1016/j.engfailanal.2014.05.024.

487 [12] K.-S. Lee, H.-J. Bang, A study on the prediction of lateral buckling load for wind turbine tower
488 structures, Int. J. Precis. Eng. Manuf. 13 (2012) 1829–1836. doi:10.1007/s12541-012-0240-y.

489 [13] J.-S. Chou, W.-T. Tu, Failure analysis and risk management of a collapsed large wind turbine
490 tower, Eng. Fail. Anal. 18 (2011) 295–313. doi:10.1016/j.engfailanal.2010.09.008.

491 [14] J.M. Adam, F.J. Pallares, Special Issue Learning from Structural failures, Eng. Struct. 32 (2010)
492 1791. doi:10.1016/j.engstruct.2010.04.026.

493 [15] N. Delatte, Failure literacy in structural engineering, Eng. Struct. 32 (2010) 1952–1954.
494 doi:10.1016/j.engstruct.2009.12.015.

495 [16] M. Currie, M. Saafi, C. Tachtatzis, F. Quail, Structural integrity monitoring of onshore wind
496 turbine concrete foundations, Renew. Energy. 83 (2015) 1131–1138.
497 doi:10.1016/j.renene.2015.05.006.

498 [17] Installing and Assembling Wind Turbine Towers, (n.d.). http://drømstørre.dk/wp-
499 content/wind/miller/windpower web/en/tour/manu/towrassy.htm (accessed August 9, 2016).

500 [18] UNE-EN 10025-3. Hot rolled products of structural steels. Part 3: Technical delivery conditions
501 for normalized rolled weldable fine grain structural steels, 2006.

502 [19] O.F. Higuera Cobos, J.F. Arroyave Londoño, C. Jaramillo I., Estudio de la fragilidad en azul del
503 acero de ultra-alta resistencia assab supra 709., Sci. Tech. ISSN 0122-1701, Vol. 3, Nº. 40, 2008,
504 Págs. 60-64. 3 (2008) 60–64.

505 [20] N. Pazos Peinado, Tecnología de los Metales y Procesos de Manufactura, Universida, Caracas,
506 2006.

507 [21] W.Y. Chu, Y.B. Wang, L.J. Qiao, Interaction between blue brittleness and stress corrosion
508 cracking, J. Nucl. Mater. 280 (2000) 250–254. doi:10.1016/S0022-3115(00)00065-9.

509 [22] M.C.S.W. Xue, The blue brittleness of 1Cr17Ni2 steel submarine motor shaft, Mater. Lett. 57
510 (2002) 369–373. doi:10.1016/S0167-577X(02)00794-2.

511 [23] H. Cui, W. Wang, A. Li, M. Li, S. Xu, H. Liu, Failure analysis of the brittle fracture of a thick-
512 walled 20 steel pipe in an ammonia synthesis unit, Eng. Fail. Anal. 17 (2010) 1359–1376.
513 doi:10.1016/j.engfailanal.2010.04.002.

514 [24] UNE 7475-1:1992. Metallic materials Charpy impact test. Part 1: Test method, 1992.

515 [25] UNE-EN 10025-2:2006. Hot rolled products of structural steels - Part 2: Technical delivery
516 conditions for non-alloy structural steels., 2006.

517   [26]   O.C. Zeinkiewick, C. Y.K., The finite element method in structural and continuum mechanics,
518   McGraw Hill, London, 1967.

519   [27]   M. E., G. I., The Finite Element Method and Applications in Engineering using ANSYS,
520   Springer, Berlin, 2005.

521   [28]   S. Moaveni, Finite Element Analysi: Theory and Application with ANSYS, Prentice-Hall, New
522   York, 2007.

523   [29]   S.A. System, ANSYS. User's manual: procedures, commands and elements., Canonsburg, PA,
524   2005.

525   [30]   J.C. Simo, T.A. Laursen, An augmented lagrangian treatment of contact problems involving
526   friction, Comput. Struct. 42 (1992) 97–116. doi:10.1016/0045-7949(92)90540-G.

527   [31]   R. Rafiee, M. Tahani, M. Moradi, Simulation of aeroelastic behavior in a composite wind turbine
528   blade, J. Wind Eng. Ind. Aerodyn. 151 (2016) 60–69. doi:10.1016/J.JWEIA.2016.01.010.

529   [32]   R. Rafiee, M. Moradi, M. Khanpour, The influence of material properties on the aeroelastic
530   behavior of a composite wind turbine blade, J. Renew. Sustain. Energy. 8 (2016) 063305.
531   doi:10.1063/1.4968600.

532   [33]   The Royal Academy of Engineering, Wind Turbine Power Calculations RWE npower
533   renewables Mechanical and Electrical Engineering, R. Acad. Eng. (n.d.).

534   [34]   thewindpower.net, (n.d.). http://www.thewindpower.net/turbine_es_57_ge-energy_1.5sle.php
535   (accessed December 6, 2016).

536   [35]   D. c. Montgomery, Design and Analysis of Experiments, 5th ed., 2001.

537   [36]   J.J. del Coz Díaz, P.J. García Nieto, A. Lozano Martínez-Luengas, J.L. Suárez Sierra, A study
538   of the collapse of a WWII communications antenna using numerical simulations based on design
539   of   experiments   by   FEM,   Eng.   Struct.   32   (2010)   1792–1800.
540   doi:10.1016/j.engstruct.2009.09.011.

541   [37]   J.J. del Coz Díaz, F.P. Álvarez Rabanal, P.J. García Nieto, J. Roces-García, A. Alonso-
542   Estébanez, Nonlinear buckling and failure analysis of a self-weighted metallic roof with and
543   without   skylights   by   FEM,   Eng.   Fail.   Anal.   26   (2012)   65–80.
544   doi:10.1016/j.engfailanal.2012.07.019.

545   [38]   J. José del Coz Díaz, J.M. Adam, A.L. Martínez-Luengas, F.P. Alvarez Rabanal, Collapse of a
546   Masonry Wall in an Industrial Building: Diagnosis by Numerical Modeling, J. Perform. Constr.
547   Facil. 27 (2013) 65–76. doi:10.1061/(ASCE)CF.1943-5509.0000310.
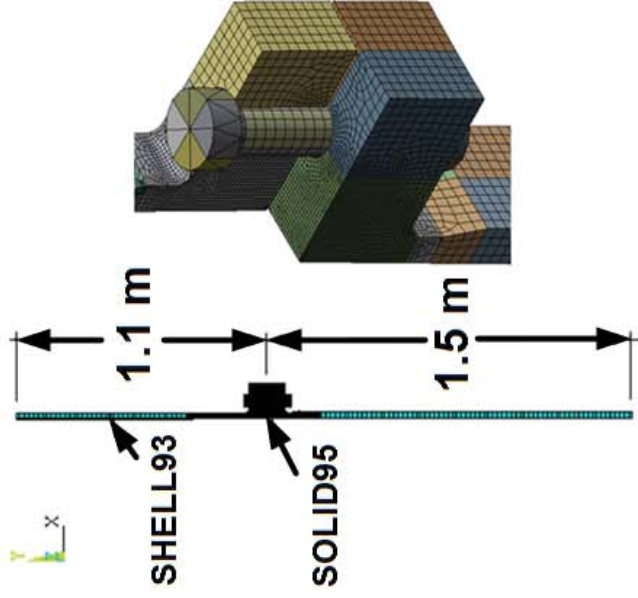
548

Highlights:

- Wind tower collapse due to the failure of a flange is analyzed
- Analysis of the material properties is needed to identify the causes of the failure
- Finite Element model shows the load distribution in the broken section
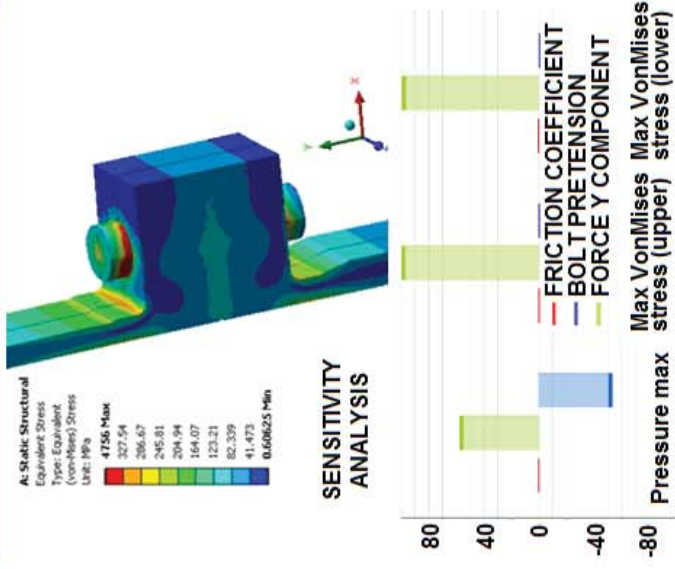- The most influential parameters are obtained applying Design of Experiments (DOE)

WIND TOWER COLLAPSE

NUMERICAL ANALYSIS

RESULTS AND DOE

SHELL93

SOLID95

1.1 m

1.5 m

A: Static Structural
Equivalent Stress
Type: Equivalent (von-Mises) Stress
Unit: MPa

4756 Max
327.54
286.67
245.81
204.94
164.07
123.21
82.339
41.473
0.60625 Min

SENSITIVITY
ANALYSIS

FRICTION COEFFICIENT
BOLT PRETENSION
FORCE Y COMPONENT

Max VonMises   Max VonMises
stress (upper)   stress (lower)

Pressure max

80   40   0   -40   -80

Wind turbine tower collapse due to flange failure: FEM and DOE analyses

Mar Alonso-Martinez [a*], José M. Adam[b], Felipe P. Alvarez-Rabanal[a],

Juan J. del Coz Díaz[a]

[a]*Department of Construction, EPSIII, University of Oviedo, 33204 Gijón, Spain*

[b]*ICITECH, Universitat Politècnica de València, Camino de Vera s/n, 46022 Valencia, Spain*

ABSTRACT

Although a large number of papers have been published to date on failures in wind turbines, most of them have focused on blade failures and less attention has been paid to the tower failures. This paper analyses the causes that led to the failure of one element that finally caused the whole tower to collapse. A diagnosis of the cause of the failure was carried out after an initial on-site inspection, when the origin of the failure appeared to be in the flange that joined the tower to its base. An experimental program was carried out to analyze the characteristics of the steel in the area nearest to the flange. A non-linear simulation was then performed by the finite element method (FEM) of the flange area where the failure had occurred, including the bolts, their prestressing forces and the contact between the joined surfaces. In order to study the influence of different variables on the flange's structural response, a method based on the Design of Experiments (DOE) was used on the FEM model. Finally, the main lessons learnt from the experience are given with the aim of contributing to improving the design and construction of wind turbine towers.

Keywords: Wind tower; Collapse; Failure; Design of experiments; Finite element modeling

* Corresponding author: Mar Alonso-Martinez

E-mail address: mar@constru.uniovi.es

Postal address: EDO 7. Room 7.1.28.

Campus de Viesques. Gijon. Asturias

CP: 33204. Spain

1. Introduction

The development of alternative sources of energy to fossil fuels has made steady progress since the world energy crisis of the seventies and has expanded with the search for clean forms of renewable energy, of which wind power has played an important role, due to its technology, infrastructure and relatively low cost [1].

Wind power is produced by using the action of the wind on an electric generator known as a wind turbine, whose main parts are the rotor blades moved by the wind, joined to an electric generator incorporating specific system management components for generating and transmitting electricity. All the equipment is supported by a tower held in place on its foundations.

In order to increase the efficiency of wind turbines, the size of these towers has continually grown throughout the years [1, 2]. The 2-3 MW wind turbines that used to dominate the market have been replaced by those of 3-5 MW [1].

At the present time most of the towers are constructed of steel tubes. The first models were built with steel lattices, but as they grew in size this system was considered inappropriate and they were replaced by the steel tubes now in use. These tower tubes are usually manufactured in two or three segments that are joined together on site, either by bolts and flanges or by welding.

The ever-increasing size of the wind turbines have meant that static calculation methods, which assumed a constant wind speed, have been replaced by dynamic simulation software that allows the aero-elastic response of the complete wind turbine to be simulated with variable dynamic loads, including the tower, the drivetrain, the rotor blades and the control system [1].

The complexity of the wind turbine structures and its components has also been the cause of a number of serious accidents. These wind turbines are generally, though not always; in the form of wind farms situated in open spaces far from residential areas. When they are close to infrastructures and built-up areas they may be a serious risk.

Wind turbine failure is often due to the failure of rotor blades or of the steel tower [3, 4]. Many papers have been published on blade failures containing simulation by numerical methods or experimental tests [4–11]. When the tower collapses it can cause serious damage to property entailing financial losses and may be due to diverse causes, one of which is the buckling of the steel tower, as pointed out in Lee & Bang [12]. Other possible causes include steel fatigue due to vibration or being shaken by the wind, failure or incorrect placement of the bolts in the base of the structure or in the joints between the different steel tube sections, as described in Chou & Tu [13].

The investigation and study of real failures can provide important information for the improvement of the design of structural elements based on new theories, concepts, construction details, monitoring, etc. [14-16]. The reason for publishing the present study was because only a few papers have been published on the particular case of wind turbine towers. The paper is organized as follows: firstly, the main characteristics of a wind turbine are given, followed by the description of the collapse of one of these structures due to the failure of the tower. The causes of the failure were determined by: visual inspection, laboratory tests, a Finite Element Method (FEM) simulation of the zone in which the failure occurred, and a Design of Experiments (DOE) to assess the influence of the different parameters involved in the

71 risk of structural collapse. In the final section, the lessons learnt from the study are given with the aim

72 of contributing to improving the design and construction of wind turbine towers.

73

74 2. Description of the wind turbine

75 The *Abuela de Santa Ana* onshore wind farm is located near the town of Pozo Llorente in the province

76 of Albacete (Spain). It consists of 25 GE Energy 1.5sle Model 1.5KW wind turbines, the diameter of

77 the rotor is 77m and the height of the tower varies between 61.4m and 85m. It is operational at the

78 present time under the control of the ACS Company at a nominal power of 37.500 kW. Its geographic

79 coordinates are 39° 4' 36.5" latitude and -1° 30' 23.5" longitude. A view of the wind farm with a close-up

80 of a tower can be seen in Fig. 1.

81 *Fig. 1.   General view of the Abuela de Santa Ana wind farm and one of the towers*

82 The turbine towers are composed of different steel tubes and the flange is fixed to the lower tube and is

83 embedded in the foundations (see Fig.2). The tower tubes are bolted together and are required to

84 maintain the necessary stiffness to support the turbine nacelles fixed to the top of the tower.

85 The flange is placed in the lower part of the tower. The flange is a steel tube 1.67 m long and 4.3 m

86 diameter. It consists of the following components (see Fig. 2):

87   - Lower T-flange to transmit loads to the foundations.

88   - Upper flange fixed to the next tower section by M36a bolts.

89 *Fig. 2.   Details of the tower/foundation connection. a) Detail of lower flange and foundation;*
90 *b) Detail of flange and bolts. Source: [17]*

91 The lower tube is totally embedded in concrete except for the upper 0.2 m which are available for

92 bolting to the tower shell. Due to its failure, the flange in one of the towers between the foundations

93 and the structure was the object of the present study.

94

95 3. Collapse of the turbine tower

96 In October 2008, two months after being out into operation, one of the *Abuela de Santa Ana* wind

97 turbine towers collapsed due to a catastrophic failure in the lower flange fixed to the foundations. An

98 on-site inspection of the damage was made the following day.

99 Firstly, the joint between the tower and the nacelle was seen to be in good condition with no evidence

100 of damage at this location having caused the failure. Secondly, the steel tube was buckled, as can be

101 seen in Fig. 3. Thirdly, the blades were seen to have damaged the steel tubes during the fall. After the

102 inspection, the most probable cause was therefore identified as the failure of the base of the tower,

103 which was made the focus of future tests to find the definite cause of the collapse.

104 *Fig. 3.   View of the tower the day after collapsing*

105 After the base had been analyzed in greater detail, the failure was located in the lower flange. This

106 component had been built from a bar of rectangular cross-section, curved and welded S-355-J2 steel

107   according to the UNE-EN-10025-3:2006 code [18] and in the zone of the failure had been welded to a
108   steel tube.

109   *Fig. 4.   View of the section in which the failure began*

110   The damaged zone (See Fig.4) showed signs of corrosion, which would later be analyzed to identify
111   the type of failure and its causes. This section was covered with a plastic sheet in order to keep these
112   zones intact and avoid any deterioration in the material due to the weather subsequent to the collapse
113   that could possibly lead to errors in the conclusions of the analysis.

114   The preliminary visual study identified a sector of approximately 3 m. that had been badly affected by
115   black, blue and brown colored oxidation, in contrast to the rest of the section in which the surface was
116   seen to be clean (Fig.4).

117

118   **4. Analysis of the collapse**

119   *4.1. Visual inspection of the broken section*

120   A scheme of the flange studied in this work can be seen in Fig. 5. The flange had been positioned in
121   order of the drill holes numbered from 1 to 138, number 1 being at the centre of the lower tower access
122   door. The broken section to be studied in detail was joined to the flange whose scheme is shown in Fig.
123   5.

124   *Fig. 5.   Detail of the flange and position of the cracks*

125   The broken section was found to have started and propagated in the base of the flange neck (see Fig.6a).
126   In photographs taken days after the collapse, various cracks were located in the flange cross-section, as
127   can be seen in Fig. 6:

128   -   The initial crack was located between drill holes 100 and 130 (see Fig.6c)
129   -   Between drill holes 109 and 123 black and blue rust stains were observed (see Fig.6b). These
130   stains were visible in the on-site inspection and were thus assumed to exist before the collapse
131   of the structure.

132   In view of the above, the start of the break was considered to date approximately from the time when
133   the tower had been constructed, due to the oxidation in the broken section.

134   The failure mode observed in the flange provided information to make a preliminary diagnosis of the
135   collapse that would later be verified by experimental tests and numerical analysis. This diagnosis
136   identified the initial crack that did not spread any further and that could have been due to the forces
137   induced by the bolt pretension or also possibly by a crack in the flange due to an impact during its
138   installation in the tower.

139   *Fig. 6.   Detail of the damaged flange section. a) Side view; b) Top view; c) Detail of crack*
140   *start point*

141   The detailed analysis of the oxides found in the damaged section included a large amount of blue oxides
142   organized into bands or groups of points (see Fig. 6c and Fig. 7) characteristic of the so-called *blue*

brittleness or *brittle martensite.* The former is often found in most steels and is due to the transformation of austenite into cementite at the grain boundaries when the material is subjected to temperatures around 300º C. The decomposition of the austenite seriously reduces the toughness of the material. This type of brittleness is accentuated by the segregation of impurities at the grain boundary, which promotes the intergranular breaks typical of brittle fractures [19] and [20]. Some authors have observed that blue brittleness when combined with corrosion cracks can cause disastrous failures in steel components [21–23].

Fig. 7.   Detail of the broken flange section

From the initial analysis based on measurements taken on site and a visual inspection, it was considered that the failed flange could have been the determining factor in the collapse of the tower. Details of the flange manufacturing process are given in the following section.

4.2. Flange manufacturing process

The flange dimensions are as follows: 4.3 m. external diameter, 0.107 m. maximum thickness, and 0.15 m. in width, with 138 drill holes of 0.039 m. in diameter. The section geometry and tolerances are given in Fig. 8.

Fig. 8.   Geometry of flange section

The flange was made from a rectangular section S-355-J2 steel bar (dimensions: 4.3x0.17x0.12 mxmxm) according to UNE-EN 10025-3:2006 [18]. The first treatment is the normalizing, after which it is cold formed and welded. The next step is the thermal treatment to eliminate any residual stresses after cold-forming. In the final stage it is machined into the required shape within the necessary tolerances. Mechanical properties of this material are well known. Quality tests were done by the steel manufacturer to ensure the material properties of the project requirements.

5. Experimental tests

In view of the type of failure discovered in the flange, close to the welded zone, the material was analyzed to obtain the fracture toughness parameters. Three Charpy specimens were extracted from the flange between drill holes 112 and 114, as shown in Fig. 9 [24].

Fig. 9.   Detail of the specimen extraction zone. Source [24]

The tests gave mean toughness values of 13 Joules for specimen W (working direction), i.e. in the direction of the tower generatrix (direction of tensile stresses in the flange when the structure is subjected to bending forces), and 10 joules for specimen M (manufacturing direction), i.e. longitudinal direction of laminated bar from which the flange is formed, as shown in Table 1.

Table 1.   Experimental Results

	Sy (MPa)	Su (MPa)	A (%)	Kv (+13ºC) (J)	Kv (-20ºC) (J)
Flange W (*)	422	557	24	62	13
Flange M (**)	383	536	28	---	10
S355 J2	>295	450-600	>18	---	>27

(*) W: Working direction

(**) M: Manufacturing direction

Reference values obtained for S355J2 grade with 105 mm width from UNE-EN 10025-2 [25].

Yield strength (Sy), Tensile Strenght (Su), Deformation (A), Toughness (Kv)

178

179 Since the value was below the 27 J given in the EN10025-3 Code [18], it was therefore concluded that
180 the fracture toughness of the material was unsatisfactory in all directions. In view of these results, a
181 serious weakness was identified in the material that could have been responsible for unforeseeable
182 failures in the behavior of the structure. The experimental results show that the material does not possess
183 the properties required by the current code and this anomaly could have caused the abnormal behavior
184 of the structure that had not been considered in its design.

185

186 **6. Finite element modelling**

187 In the present work, a numerical model based on Finite Element Method studied the behavior of the
188 flange in order to analyze the cause of the collapse. The procedure followed in this stage consisting of
189 a detailed geometrical model of a sector of the flange, taking advantage of its symmetry. The upper and
190 lower steel tubes were included, as were the zones affected by welding and the bolts.

191 FEM makes it possible to calculate strains and stresses and the possible failure modes under a range of
192 stresses and working conditions [26]. Ansys-Workbench R16.1 Academic software [27] and [28] was
193 used for this study.

194 The analyses were supplemented by a design of experiments (DOE) study (see Section 7) in which the
195 influence of the different input variables was assessed to identify the response of the flange under
196 different conditions.

197

198 *6.1. Material properties and geometry*

199 The materials were modelled considering the steel's elastic properties with linear behavior until
200 yielding. The defined material was steel with a modulus of elasticity of 200 GPa and a Poisson's
201 Coefficient of 0.3, yield strength of 250 MPa and ultimate tensile strength of 460 MPa. These properties
202 have been taken from the manufacturer datasheet.

203 The geometrical model studied consisted of the lower flange, the upper flange and a bolt joining both
204 parts, to which symmetry conditions were applied in order to reduce the computational cost of the
205 models. Details of the model geometry can be seen in Fig. 10.

206 *Fig. 10.   Geometric model: a) Lower flange; b) Upper flange and bolt; c) Complete*
207 *(symmetry) model.*

208

6.2. Finite elements used and contact model

210 SOLID95 type finite elements were used for the flange and SHELL93 for the steel tube at a distance
211 from the joint (see Fig.11a). These elements are suitable for modelling curved zones and complex
212 geometries, as in the case under study [25–27].

213 SOLID95 is a 3-D element with 20 nodes and three degrees of freedom able to accurately simulate
214 irregular geometries and structural phenomena such as plasticity, creep and large deformations, among
215 others [29].

216 SHELL93 is an element defined by 8 nodes and three degrees of freedom in each node (displacement
217 and rotations in three directions of the space) and is suitable for curved plate models such as the steel
218 tube at a distance from the joint in the present study [29].

219 The mesh size was minimum 0.0013 m and maximum 0.27 m, with a total of 266.194 nodes and 71.117
220 elements. As can be seen in Figure 11b, certain zones of the geometry were modelled with a very fine
221 finite elements mesh due to the curves and transitions between the elements.

222 *Fig. 11.   Finite elements mesh: a) General view; b) Detail of the mesh in the bolt*
223 In this case, the average element quality ratio is 0.806 out of 1. In consequence, numerical results are
224 in good agreement with the expected behavior. For three-dimensional elements, this metric is based on
225 the ratio of the volume to the sum of the square root of the sum of the square of the edge lengths.

226 The model was completed with the configuration of the contact between elements and the application
227 of boundary conditions, which consisted of frictional contact between the flanges surfaces and bonded
228 contact between the bolt head and the upper flange surfaces and for the nut with the lower flange
229 surfaces (see Fig.12). The friction coefficient considered was 0.1, adopting an Augmented Lagrangian
230 formulation [30].

231 *Fig. 12.   Contacts in model*

232

6.3. Loads and boundary conditions

234 This section provides details of the loads applied to the finite element (FE) model and the boundary
235 conditions considered for the joint as well as the simplification procedure in order to obtain realistic
236 values and structural response from the engineering point of view.

237 To begin with, use was made of the flange symmetry to simplify the model and represent the actual
238 continuity of the tower shell and flanges. In this way, only a 1/138th sector of the flange was simulated
239 and symmetry conditions were applied (see Fig. 13). Secondly, a restriction was applied on the

240 displacements at the lower end of the foundation steel tube (A in Fig. 13). Thirdly, a load was applied
241 on the upper end of the joint (B in Fig. 13) representing the vertical load exerted on the foundation by
242 the structure and its various components. Additionally, other loads present in the structure were applied,
243 whose values were provided by the manufacturer of the tower (C and D in Fig. 13). The loads applied
244 on the model and their values (see Fig. 13) were as follows:

245 - Fixed support on the base of the foundation steel tube (A in Fig. 13).
246 - Compression load on the upper steel tube of the flange to the value of 32.57 kN (B in Fig. 13).
247 - Load applied on all the steel tube in a direction perpendicular to the axis of the tower
248   corresponding to the maximum wind pressure on the structure, whose value is $1{,}236 \cdot 10^{-3}$ MPa
249   (C in Fig. 13).
250 - A pretension load applied on the bolt joining the upper and lower flanges at a value of 519.91kN
251   (D in Fig. 13).

252 The force generated by the wind on the blades causes a bending moment at the base of the tower that
253 subjects the joint to tensile and compressive forces. There are several ways to obtain the wind load on
254 the blades [13], [10]. The use of Computer Fluid Dynamics (CFD) is a useful methodology to obtain
255 the wind load on blades including the aeroelastic behavior. Other authors used this methodology in the
256 last years [31]. Furthermore, the influence of the blade material properties on the tower wind load could
257 be taking into account [32]

258 In the present work, the load is obtained following the standards and guides as follows [33]. This
259 horizontal force is limited by the available power, P_a. The available power is obtained by applying a
260 correcting ratio to the power generated due to the kinetic energy of the wind, P (see Eq. (1)). The
261 maximum efficient power of a turbine is restricted by the Betz Limit, which is called the "power
262 coefficient", C_p [33]. Betz's Law defines this coefficient for any design of wind turbine at 0.59. Despite
263 the fact that Betz Law establishes the theoretical maximum power efficiency at 59%, other factors such
264 as strength or durability reduce this value to 0.35 – 0.45. Usually, for high performance equipment, the
265 Betz limit value considered is 0.4.

266 $P_a = C_p \cdot P$ Eq. (1)

267 The power generated is determined by the kinetic energy of the wind in accordance with Eq. (2).

268 $P = \frac{1}{2} \cdot \rho \cdot A \cdot v^3$ Eq. (2)

269 Where:

270 ρ: Air density in kg/m^3

271 A: Area swept by rotor in m^2

272 v: Linear velocity of the wind in m/s

273 The horizontal force on the rotor is determined by Eq. (3).

274 $F = \frac{P_a}{v} = \frac{C_p \cdot P_d}{v}$ Eq. (3)

275 Data on the characteristics of the rotor are required for calculating the horizontal force. The
276 characteristics are specified in Table 2.

277

282 Table 2.   Wind turbine information

Wind power component	Values
Rotor diameter, D (m)	77
Swept area, A (m^2)	4 656.6
Nacelle weight, (kg)	50 000
Rotor + hub weight (kg)	31 000
Wind Speed, v (m/s)	5.21

279

280 The values obtained for the power and for the horizontal force on the rotor are shown in Table 3.

281

282 Table 3.   Power and load on the wind turbine.

Loads	Values
Power (kW)	742.41
Avaliable Power (kW)	296.96
Wind force (kN)	46.57

283

284 The maximum tensile stress on the tower flange is due to two main forces (see Eq. (4)):

285   -   The bending moment caused by the horizontal force of the wind on the rotor.
286   -   The weight of the turbine unit and the tower, which generate a normal force on the flange.

287 $$\sigma_{\max (c)} = \frac{M_f}{W_f} + \frac{P_p}{S}$$ Eq. (4)

288 Where:

289 M_f: Bending moment on the tower flange (kN·m)

290 W_f: Bending resistance (m^3)

291 P_p: Self-weight (kN)

292 S: Cross-section area of the tower (m^2)

293 The bending moment in the tower flange is obtained by multiplying the horizontal force on the rotor by
294 the distance to the base of the tower (Eq. (5)).

295 $M_f = F \cdot d \cdot \gamma$ Eq. (5)

296 Where:

297 F: Horizontal force generated by the wind (kN)

298 d: Distance to the base of the tower, 80 m.

299 γ: Safety factor, 1.5

300 To calculate the self-weight, the weight of the tower ($P_{w\text{-}tower}$) and the weight of the turbine unit ($P_{w\text{-}turbine}$) comprising the nacelle, rotor and hub must all be taken into consideration (Eq. (6)). Data
301 necessary to obtain $P_{w\text{-}tower}$ and $P_{w\text{-}turbine}$ are shown in Table 2.
302

303 $P_p = P_{w-tower} + P_{w-turbine}$ Eq. (6)

304 The weight of the tower ($P_{w\text{-}tower}$) is 169.67 kN, and the weight of the wind turbine ($P_{w\text{-}turbine}$) is 810 kN,
305 including the nacelle, rotor and hub[34]. Therefore, the self-weight of the wind turbine (P_p) is 979.67
306 kN.

307 By using these data, the maximum stress on the flange can be expressed by Eq. (4), while the minimum
308 stress can be determined by the tensile stress on the flange (Eq. (7)).

309 $\sigma_{\min (t)} = \dfrac{M}{W_f} - \dfrac{P_p}{S}$ Eq. (7)

310 The stress values on the flange are shown in Table 4.

311 Table 4.   Stress values on the flange

Stress	
Max. Compression Stress $\sigma_{\max (c)}$ (MPa)	16.64
Max. Tensile Stress $\sigma_{\max (t)}$ (MPa)	9.38
Max. Compressive load (kN)	(-)32.57
Tensile Load (kN)	(+)18.37

312

313 Based on the results obtained, the normal load applied to the flange was varied between 15 kN of
314 maximum tensile load and 40 kN of maximum compressive load for the study of all the states of
315 intermediate loads between the maximum load (compressive) and the minimum load (tensile).

316   *Fig. 13.   Boundary conditions used on a section of the flange*

317 The computational calculation was performed by means of the Newton-Raphson iterative method,
318 based firstly on the pretension analysis of the bolt with a subsequent application of all the loads required
319 by the flange. The pretension load is modelled using a set of pretension elements (element type
320 PRETS179), [28]. This element has one translation degree of freedom, which is the pretension direction.
321 The surfaces connected by the pretension elements must be matched using coincident nodes in both
322 meshes to obtain accurate results. A total of 8 sub-steps and 17 iterations were necessary before model
323 convergence was achieved.

6.4. Analysis of the results

The results obtained from the numerical simulations provided interesting information for an exhaustive analysis of the tower failure. On analyzing the stresses in the joint it was seen that the prestressing of the bolts, before considering the other loads, exerts high forces on the joint, as can be seen in Fig. 14a, since the flange steel's yield strength is exceeded. As a result, the flange is already in a highly stressed state even before the other loads on the structure are taken into account.

After applying loads on the structure, the numerical model showed a high concentration of stresses on the flange neck that coincided with the point of the failure observed in the visual inspection. After analyzing the results of the numerical model, it is shown that the Maximum Von-Mises stress exceeded the material's yield strength (see Fig.14b).

Fig. 14 gives the most important results of the Von Mises stress distribution in the flange. Fig. 14a shows the stress state of the joint when subjected to bolt pretension only. Fig. 14b includes the stress state of the flange when subjected to all the loads.

Fig. 14. *FEM model results, equivalent Von-Mises stress. a) applying bolt pretension only (in MPa); b) for all applied loads (in MPa)*

7. Design of experiments (DOE)

7.1. General information

Design of Experiments (DOE) is a technique used to identify the influence of input parameters on output parameters, as well as to optimize the analysis results. This technique is widely used in engineering to obtain results from a range of input parameters using a minimum of input sampling points. Response surface provide intermediate results. The accuracy of the response surface depends on the type of DOE and the number of cases studied, [35].

In this work, a DOE, type Central Composite Design (CCD), was used to study the influence of certain conditions on the level of stresses in each part of the flange section. This method was used by the authors in previous work on the analysis of structural failures and to optimize new designs [32–34].

In this case, the focus was on the flange bolt pretension, the coefficient of friction in the flange contact, and the vertical force on the flange, which could affect the structural integrity of the joint. The output parameters studied were the maximum stress on the[35] joint and the maximum Von Mises stress in the analysis. Table 5 gives the maximum values adopted for the input variables and their initial values.

Table 5. Values of parameters in the DOE

	Minimum Value	Initial Value	Maximum Value
Frictional Coefficient	0.1	0.1	0.3
Bolt preload (kN)	100	520	571
Force (Y axis) (kN)	-40	32.5	15

358 The analysis identified the individual critical stress values for each element under different load states.
359 The results obtained allowed us to identify the most important critical points in the joint, the influence
360 of the input variables on each one, and the permitted load limits to keep the structure in a state of stress
361 within the material's admissible limits.

362 The DOE analysis can identify the cause of the fracture of the joint, the load limits that would cause the
363 collapse of the structure and the different load combinations that would overload the joint and cause it
364 to have brittle behavior.

365

366 ## 7.2. Analysis of the results

367 The maximum stress values were the most important results obtained from the numerical analysis of
368 the joint, including the contact stress between both flanges and the individual stress level of both the
369 upper and lower flanges.

370 In regard to the flange contact pressure (see Fig.15a), the maximum value obtained was in the central
371 axis of the surface and reached a value of 62.8 MPa. The maximum Von Mises stress values in upper
372 and lower flanges were very high (see Figs. 15b and 15c).

373 *Fig. 15.   Results of the FE model and DOE analysis: a) Contact stress between upper and*
374 *lower flanges (in Pa); b) Von Mises stress in upper flange (in Pa); c) Von Mises stress in*
375 *lower flange (in Pa)*

376 The DOE results also contributed to the diagnosis of the collapse of the structure by identifying the the
377 most influential variables of the limit stress state of the joint. In the sensitivity analysis shown in Fig.
378 16, it can be seen that the most influential parameter is the pretension stress applied to the bolt, followed
379 by the vertical component of the load applied to the steel tube, and lastly the coefficient of friction
380 between the contact surfaces of the flanges.

381 *Fig. 16.   Sensitivity analysis*

382 Fig. 17 shows the response surface that reflects the variation in maximum Von Mises stress in the
383 different parts of the upper and lower flanges. In both cases the maximum Von Mises stress considered
384 was in the part nearest to the steel tube, since, as was seen previously, this is the zone of the flange with
385 the highest concentration of stresses.

386 The response surfaces obtained from the DOE had maximum values very similar to the upper and lower
387 parts of the flange. It was also seen that the bolt pretension load had a greater influence than the vertical
388 load on the steel tube in the maximum von Mises stress value.

389 *Fig. 17.   DOE analysis: External part of the flange (upper and lower part. a) Bolt pretension*
390 *vs Force Y in upper part of the flange; b) Bolt pretension vs Force Y in lower part of the*
391 *flange*

392 Fig. 18a shows the influence of the bolt pretension load and of the coefficient of friction with respect
393 to the pressure in the contact between the flanges. It can be seen that the most influential parameter is
394 the pretension load. Figure 18b shows the influence of the vertical load on the pressure value; it can be
395 seen that the greatest influence is due to the vertical load applied to the steel tube.

396 *Fig. 18.   DOE analysis: maximum pressure in contact between the flanges: a) Contact friction*
397 *vs Bolt pretension; b) Contact friction vs Force Y.*

398   Statistical parameters of this DOE are included in Table 6.

399

8. Diagnosis

401   In the visual inspection carried out on site it was determined that the failure had occurred in two phases
402   in a brief interval of time:

403   1)   The initial failure appeared to be caused by force that disappeared after the crack started
404   (a case of imposed deformation and/or a temporary force derived from an undue event).
405   After this study, it was considered that the failure occurred during the building of the
406   turbine tower, when the pretension was applied to the bolts.
407   2)   The second failure occurred when the tower was in service and the resistant section
408   became weakened because of the initial fracture and progressed until the tower
409   collapsed.

410   The presence of blue oxides in the fracture zone indicated the possibility of a defect in the manufacture
411   of the element. To verify this, experimental tests were carried out on the toughness of the steel used in
412   the tower and showed that the steel did not meet the requirements of the resilience test. The steel was
413   shown to have very low toughness and was not suitable for use in the structure.

414   FEM numerical simulations and DOE were used in the present study to analyze the collapse of the wind
415   turbine tower. The results obtained showed that the pretension of the bolts, before considering the
416   remaining forces, exerted considerable stresses on the joint (Fig.14a) that reached the yield strength of
417   the steel in the flange. This high concentration of stresses occurred precisely at the fracture point in the
418   flange neck observed in the visual inspection. The sensitivity analysis by DOE (Fig.16) also showed
419   that the most influential parameter in regard to the von Mises stresses in the joint was the preload stress
420   applied to the bolts. Finally, the response surfaces obtained from the DOE analysis showed that the bolt
421   pretension load had a clearly greater influence than the vertical load and the coefficient of friction in
422   the value of the maximum von Mises stress throughout the range of loads applied to the flange.

423   Therefore, based on the visual inspection, the laboratory tests carried out and the numerical technique
424   employed (FEM models, sensitivity analysis, response surfaces and the DOE-based method) it can be
425   stated that the collapse of the tower was due to defective material combined with errors in the design of
426   the flange. Both issues make the stress due to the bolt pretension combined with the residual welding
427   stresses are higher than the strength and toughness of the flange material.

428

9. Conclusions and lessons learned

430   This paper analyze the collapse of a wind turbine tower. The causes of the failure were determined by
431   a visual inspection, laboratory tests, FEM simulations and a subsequent DOE analysis. The main lessons
432   learned can be summed up as follows:

433   1.   On-site inspection of the collapsed structure is essential, together with the immediate isolation
434   of the fractured section to avoid any changes due to oxidation or other agencies.
435   2.   The observation of the fractured section and detailed photographs of all sectors to show
436   differences in colour or appearance can also contribute to clarifying the causes of a collapse.

3. The experimental analysis of all material properties such as resistance or toughness is fundamental to establish the possible causes of the failure.
4. The creation of detailed FEM models to study the load distribution in the broken section enable the analysis of possible causes of the failure.
5. Applying the DOE technique in the study provides information on the structural behaviour when the physical properties or the loads have wide range of variations and is a fundamental tool for identifying the basic variables involved in the phenomenon.

In the present case, the failure could have been avoided if the material used in the flange had been subjected to the appropriate quality control (toughness test). It could also have been avoided had the flange been better designed to remove the maximum service stress away from the zone affected by the welding, e.g. with a larger chord radius and longer neck.

Acknowledgements

References

[1] C.C. Chia, J.-R. Lee, Hyung-Joon Bang, Structural health monitoring for a wind turbine system: a review of damage detection methods, Meas. Sci. Technol. 19 (2008) 122001. doi:10.1088/0957-0233/19/12/122001.

[2] Y. Lin, L. Tu, H. Liu, W. Li, Fault analysis of wind turbines in China, Renew. Sustain. Energy Rev. 55 (2016) 482–490. doi:10.1016/j.rser.2015.10.149.

[3] Caithness Windfarm Information Forum (CWIF), Summ. Wind Turbine Accid. Data to 30 Sept. 2014. (n.d.). http://www.caithnesswindfarms.co.uk/ (accessed August 9, 2016).

[4] F.P.G. Marquez, J.M.P. Perez, A.P. Marugan, M. Papaelias, Identification of critical components of wind turbines using FTA over the time, Renew. Energy. 87 (2016) 869–883. doi:10.1016/j.renene.2015.09.038.

[5] L.C.T. Overgaard, E. Lund, Structural collapse of a wind turbine blade. Part B: Progressive interlaminar failure models, Compos. Part A Appl. Sci. Manuf. 41 (2010) 271–283. doi:10.1016/j.compositesa.2009.10.012.

[6] M.M. Shokrieh, R. Rafiee, Simulation of fatigue failure in a full composite wind turbine blade, Compos. Struct. 74 (2006) 332–342. doi:10.1016/j.compstruct.2005.04.027.

[7] C. Kong, J. Bang, Y. Sugiyama, Structural investigation of composite wind turbine blade considering various load cases and fatigue life, Energy. 30 (2005) 2101–2114. doi:10.1016/j.energy.2004.08.016.

476 [8]   F.M. Jensen, B.G. Falzon, J. Ankersen, H. Stang, Structural testing and numerical simulation of
477   a 34m composite wind turbine blade, Compos. Struct. 76 (2006) 52–61.
478   doi:10.1016/j.compstruct.2006.06.008.

479 [9]   L.C.T. Overgaard, E. Lund, O.T. Thomsen, Structural collapse of a wind turbine blade. Part A:
480   Static test and equivalent single layered models, Compos. Part A Appl. Sci. Manuf. 41 (2010)
481   257–270. doi:10.1016/j.compositesa.2009.10.011.

482 [10] C.P. Chen, T.Y. Kam, Failure Analysis of Small Composite Sandwich Turbine Blade Subjected
483   to Extreme Wind Load, Procedia Eng. 14 (2011) 1973–1981. doi:10.1016/j.proeng.2011.07.248.

484 [11] X. Chen, W. Zhao, X.L. Zhao, J.Z. Xu, Preliminary failure investigation of a 52.3m glass/epoxy
485   composite wind turbine blade, Eng. Fail. Anal. 44 (2014) 345–350.
486   doi:10.1016/j.engfailanal.2014.05.024.

487 [12] K.-S. Lee, H.-J. Bang, A study on the prediction of lateral buckling load for wind turbine tower
488   structures, Int. J. Precis. Eng. Manuf. 13 (2012) 1829–1836. doi:10.1007/s12541-012-0240-y.

489 [13] J.-S. Chou, W.-T. Tu, Failure analysis and risk management of a collapsed large wind turbine
490   tower, Eng. Fail. Anal. 18 (2011) 295–313. doi:10.1016/j.engfailanal.2010.09.008.

491 [14] J.M. Adam, F.J. Pallares, Special Issue Learning from Structural failures, Eng. Struct. 32 (2010)
492   1791. doi:10.1016/j.engstruct.2010.04.026.

493 [15] N. Delatte, Failure literacy in structural engineering, Eng. Struct. 32 (2010) 1952–1954.
494   doi:10.1016/j.engstruct.2009.12.015.

495 [16] M. Currie, M. Saafi, C. Tachtatzis, F. Quail, Structural integrity monitoring of onshore wind
496   turbine concrete foundations, Renew. Energy. 83 (2015) 1131–1138.
497   doi:10.1016/j.renene.2015.05.006.

498 [17] Installing and Assembling Wind Turbine Towers, (n.d.). http://drømstørre.dk/wp-
499   content/wind/miller/windpower web/en/tour/manu/towrassy.htm (accessed August 9, 2016).

500 [18] UNE-EN 10025-3. Hot rolled products of structural steels. Part 3: Technical delivery conditions
501   for normalized rolled weldable fine grain structural steels, 2006.

502 [19] O.F. Higuera Cobos, J.F. Arroyave Londoño, C. Jaramillo I., Estudio de la fragilidad en azul del
503   acero de ultra-alta resistencia assab supra 709., Sci. Tech. ISSN 0122-1701, Vol. 3, Nº. 40, 2008,
504   Págs. 60-64. 3 (2008) 60–64.

505 [20] N. Pazos Peinado, Tecnología de los Metales y Procesos de Manufactura, Universida, Caracas,
506   2006.

507 [21] W.Y. Chu, Y.B. Wang, L.J. Qiao, Interaction between blue brittleness and stress corrosion
508   cracking, J. Nucl. Mater. 280 (2000) 250–254. doi:10.1016/S0022-3115(00)00065-9.

509 [22] M.C.S.W. Xue, The blue brittleness of 1Cr17Ni2 steel submarine motor shaft, Mater. Lett. 57
510   (2002) 369–373. doi:10.1016/S0167-577X(02)00794-2.

511 [23] H. Cui, W. Wang, A. Li, M. Li, S. Xu, H. Liu, Failure analysis of the brittle fracture of a thick-
512   walled 20 steel pipe in an ammonia synthesis unit, Eng. Fail. Anal. 17 (2010) 1359–1376.
513   doi:10.1016/j.engfailanal.2010.04.002.

514 [24] UNE 7475-1:1992. Metallic materials Charpy impact test. Part 1: Test method, 1992.

515 [25] UNE-EN 10025-2:2006. Hot rolled products of structural steels - Part 2: Technical delivery
516   conditions for non-alloy structural steels., 2006.

517 [26] O.C. Zeinkiewick, C. Y.K., The finite element method in structural and continuum mechanics,
518 McGraw Hill, London, 1967.

519 [27] M. E., G. I., The Finite Element Method and Applications in Engineering using ANSYS,
520 Springer, Berlin, 2005.

521 [28] S. Moaveni, Finite Element Analysi: Theory and Application with ANSYS, Prentice-Hall, New
522 York, 2007.

523 [29] S.A. System, ANSYS. User's manual: procedures, commands and elements., Canonsburg, PA,
524 2005.

525 [30] J.C. Simo, T.A. Laursen, An augmented lagrangian treatment of contact problems involving
526 friction, Comput. Struct. 42 (1992) 97–116. doi:10.1016/0045-7949(92)90540-G.

527 [31] R. Rafiee, M. Tahani, M. Moradi, Simulation of aeroelastic behavior in a composite wind turbine
528 blade, J. Wind Eng. Ind. Aerodyn. 151 (2016) 60–69. doi:10.1016/J.JWEIA.2016.01.010.

529 [32] R. Rafiee, M. Moradi, M. Khanpour, The influence of material properties on the aeroelastic
530 behavior of a composite wind turbine blade, J. Renew. Sustain. Energy. 8 (2016) 063305.
531 doi:10.1063/1.4968600.

532 [33] The Royal Academy of Engineering, Wind Turbine Power Calculations RWE npower
533 renewables Mechanical and Electrical Engineering, R. Acad. Eng. (n.d.).

534 [34] thewindpower.net, (n.d.). http://www.thewindpower.net/turbine_es_57_ge-energy_1.5sle.php
535 (accessed December 6, 2016).

536 [35] D. c. Montgomery, Design and Analysis of Experiments, 5th ed., 2001.

537 [36] J.J. del Coz Díaz, P.J. García Nieto, A. Lozano Martínez-Luengas, J.L. Suárez Sierra, A study
538 of the collapse of a WWII communications antenna using numerical simulations based on design
539 of experiments by FEM, Eng. Struct. 32 (2010) 1792–1800.
540 doi:10.1016/j.engstruct.2009.09.011.

541 [37] J.J. del Coz Díaz, F.P. Álvarez Rabanal, P.J. García Nieto, J. Roces-García, A. Alonso-
542 Estébanez, Nonlinear buckling and failure analysis of a self-weighted metallic roof with and
543 without skylights by FEM, Eng. Fail. Anal. 26 (2012) 65–80.
544 doi:10.1016/j.engfailanal.2012.07.019.

545 [38] J. José del Coz Díaz, J.M. Adam, A.L. Martínez-Luengas, F.P. Alvarez Rabanal, Collapse of a
546 Masonry Wall in an Industrial Building: Diagnosis by Numerical Modeling, J. Perform. Constr.
547 Facil. 27 (2013) 65–76. doi:10.1061/(ASCE)CF.1943-5509.0000310.

548

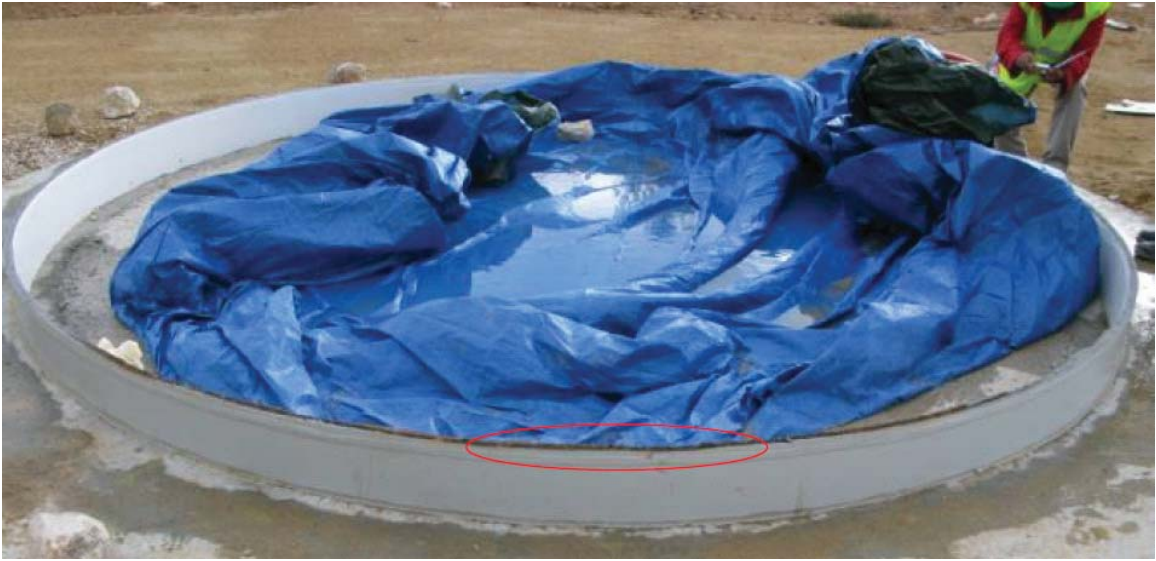*Fig. 1.   General view of the Abuela de Santa Ana wind farm and one of the towers*
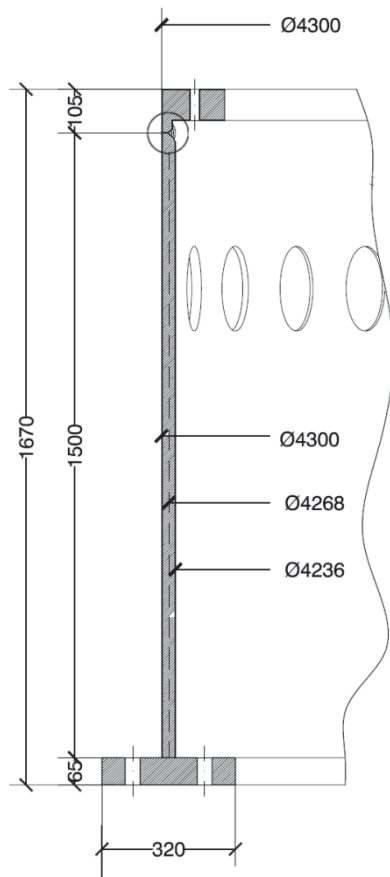
Fig. 2.   *Details of the tower/foundation connection. a) Detail of lower flange and foundation; b) Detail of flange and bolts. Source: [16]*

Fig. 3.   View of the tower the day after collapsing

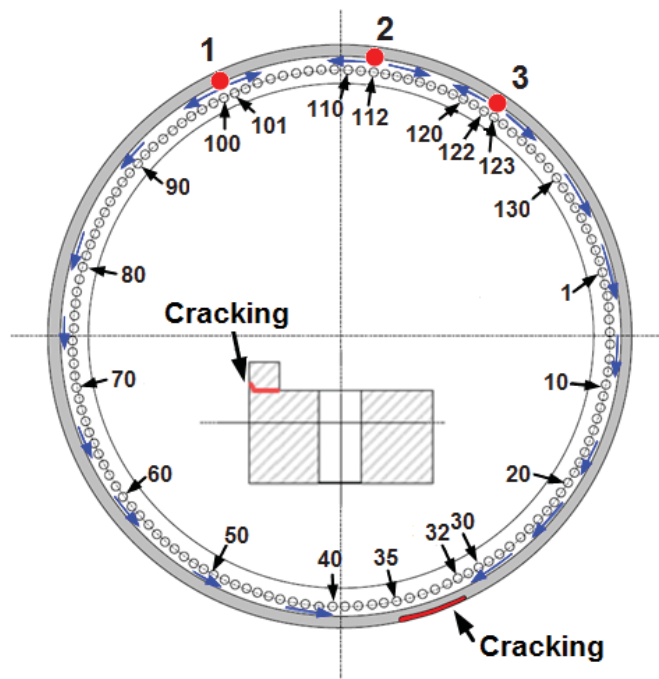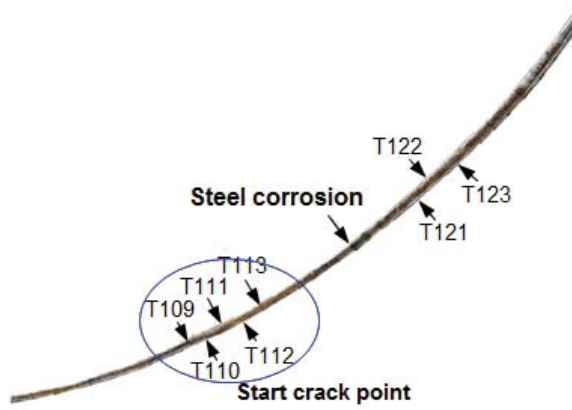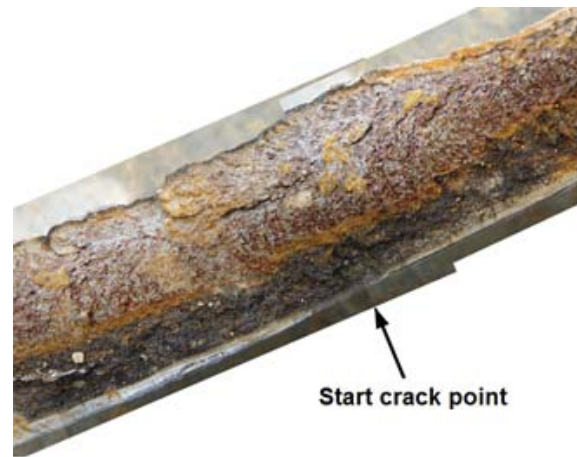*Fig. 4.   View of the section in which the failure began*

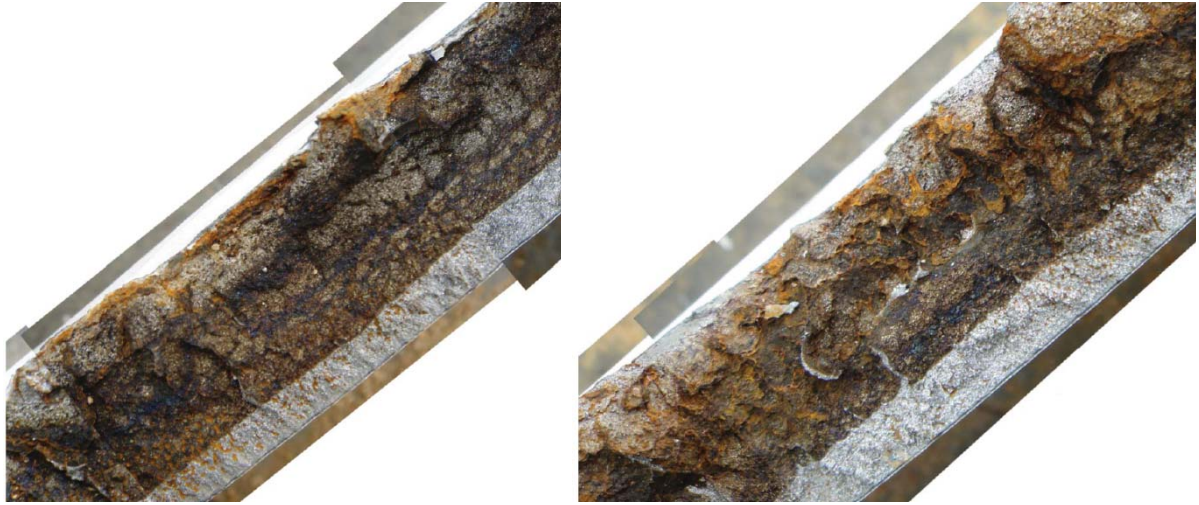*Fig. 5.   Detail of the flange and position of the cracks*

(a)

(b)

(c)

Fig. 6.   Detail of the damaged flange section. a)Side view; b) Top view; c) Detail of crack start point

Fig. 7.   Detail of the broken flange section
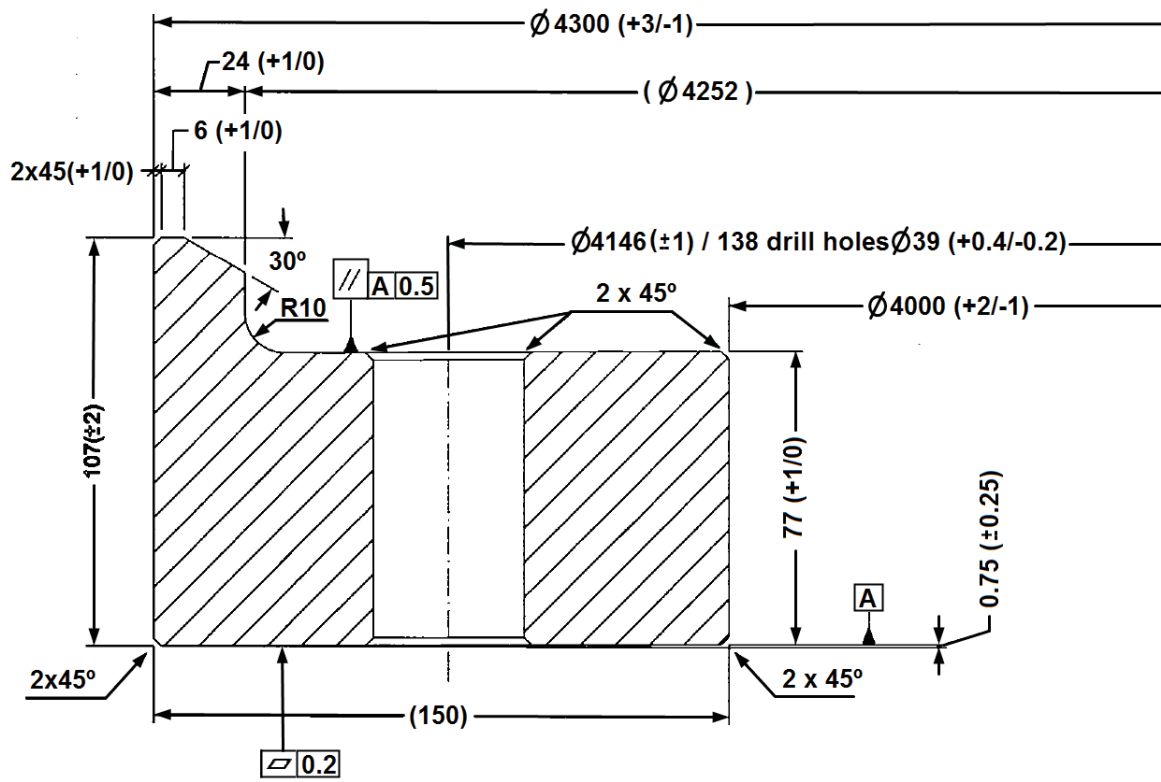
Fig. 8.   Geometry of flange section
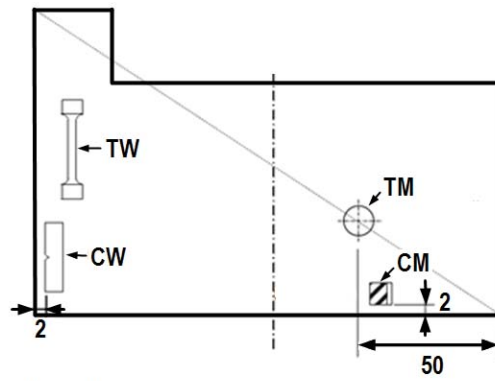
TW: Tensile specimen in working direction
CW: Charpy impact test specimen in working direction
TM: Tensile specimen in manufacturing direction
CM: Charpy impact test specimen in manufacturing direction

Fig. 9.   Detail of the specimen extraction zone [23]
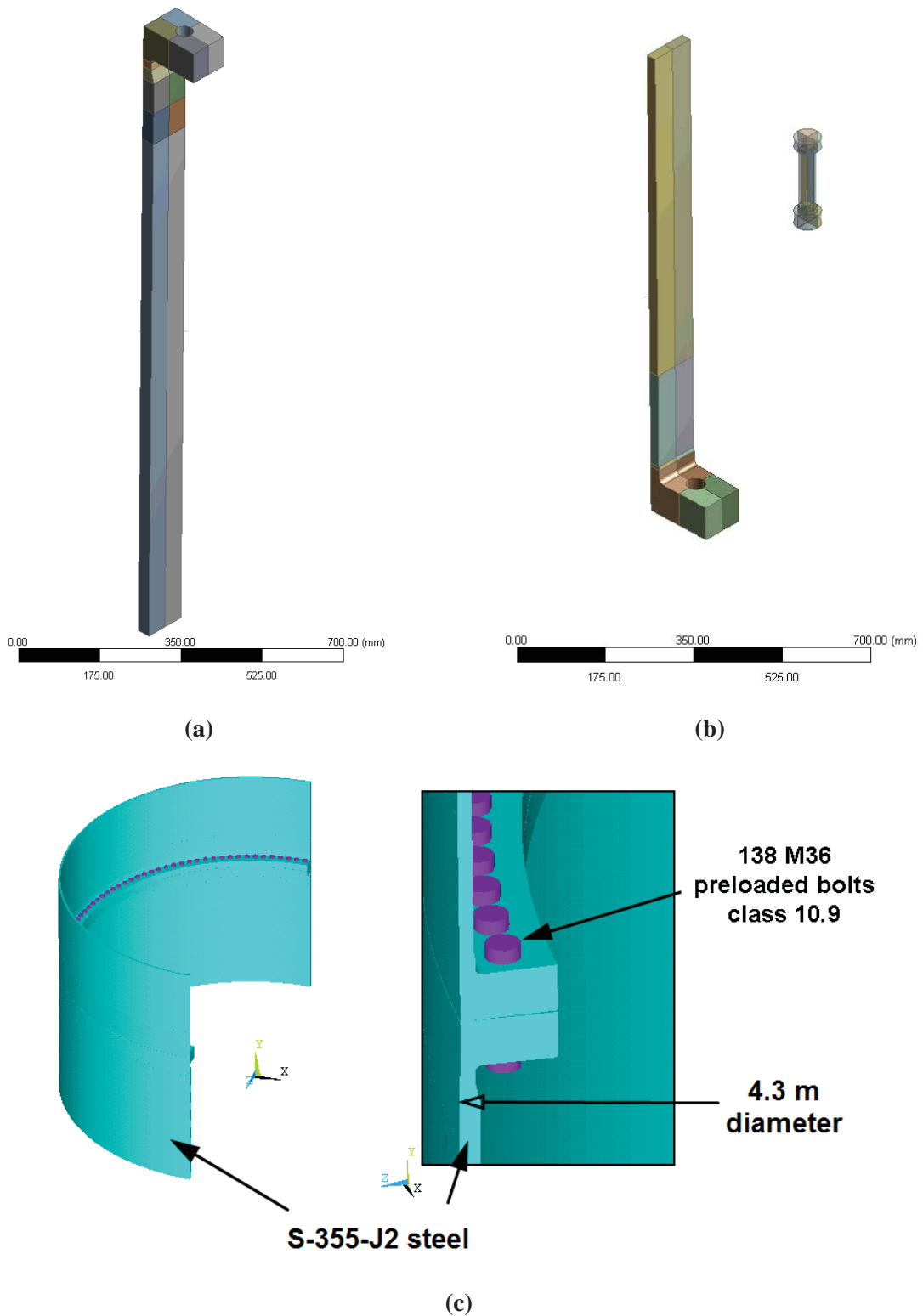
Fig. 10.   Geometric model: a) Lower flange; b) Upper flange and bolt; c) Complete (symmetry) model.

| (a) | (b) |
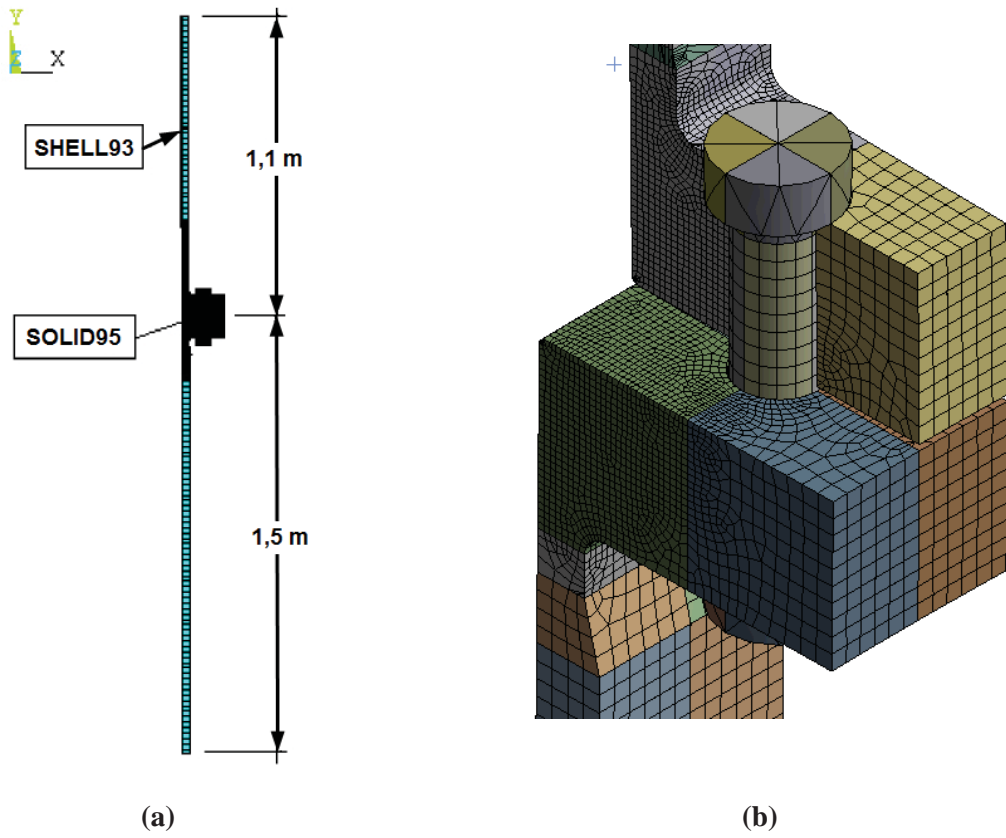
Fig. 11.   *Finite elements mesh: a) General view; b) Detail of the mesh in the bolt*
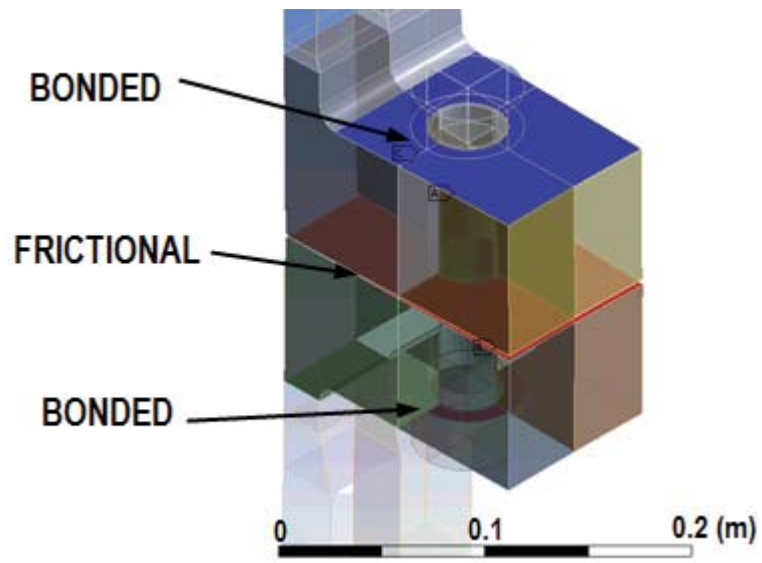
Fig. 12.   Contacts in model
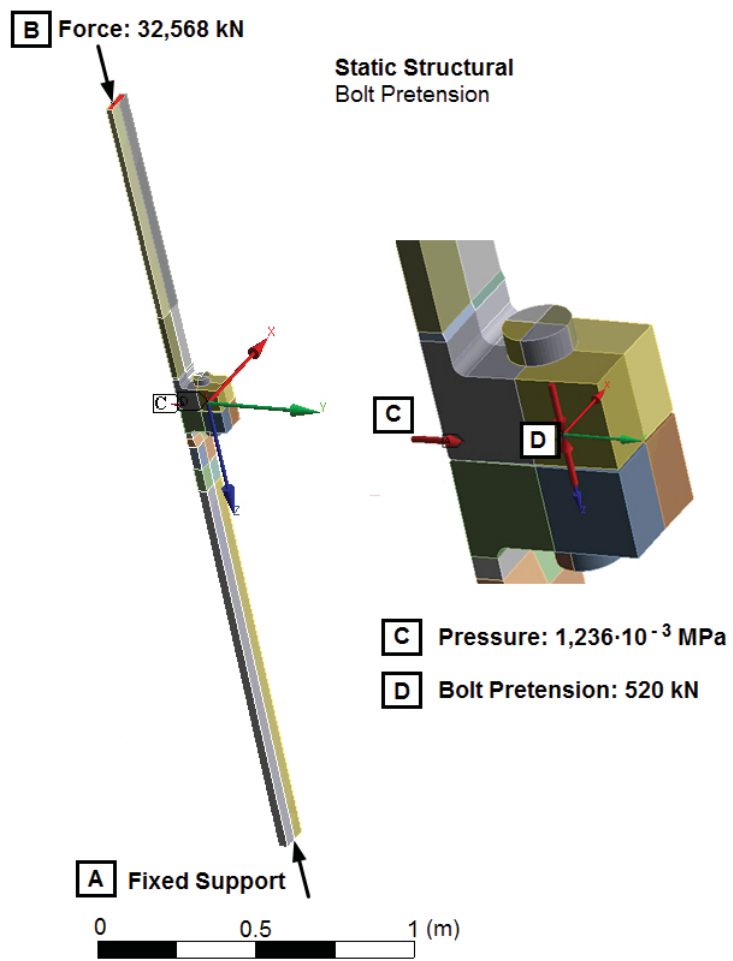
Fig. 13.   Boundary conditions used on a section of the flange
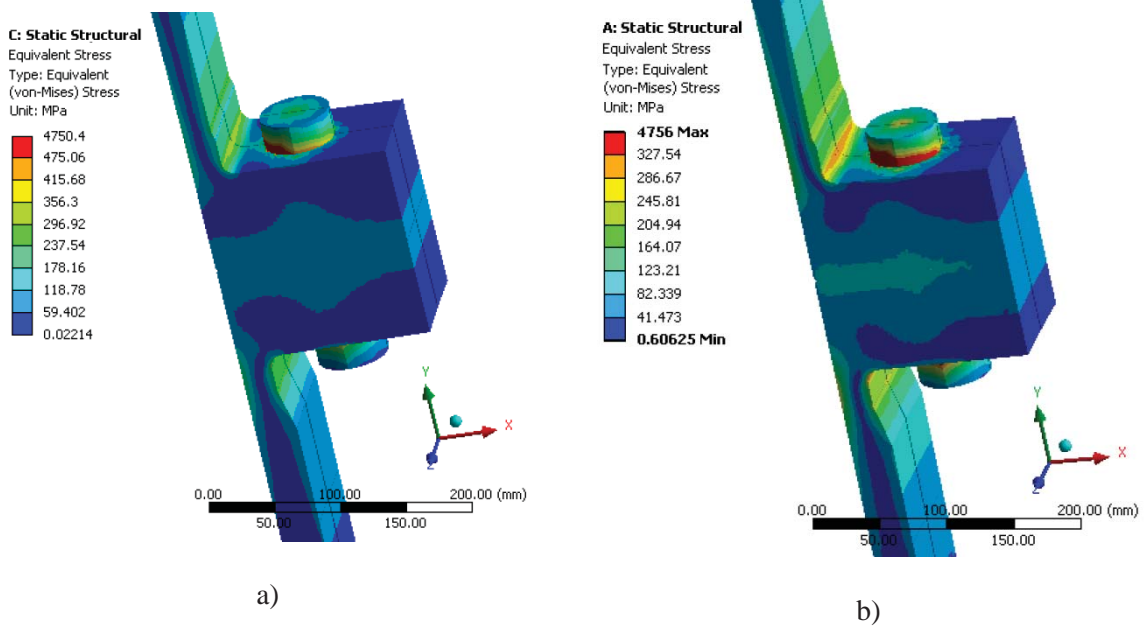
Fig. 14. FEM model results, equivalent Von-Mises stress. a) applying bolt pretension only (in Pa); b) for all applied loads (in Pa)
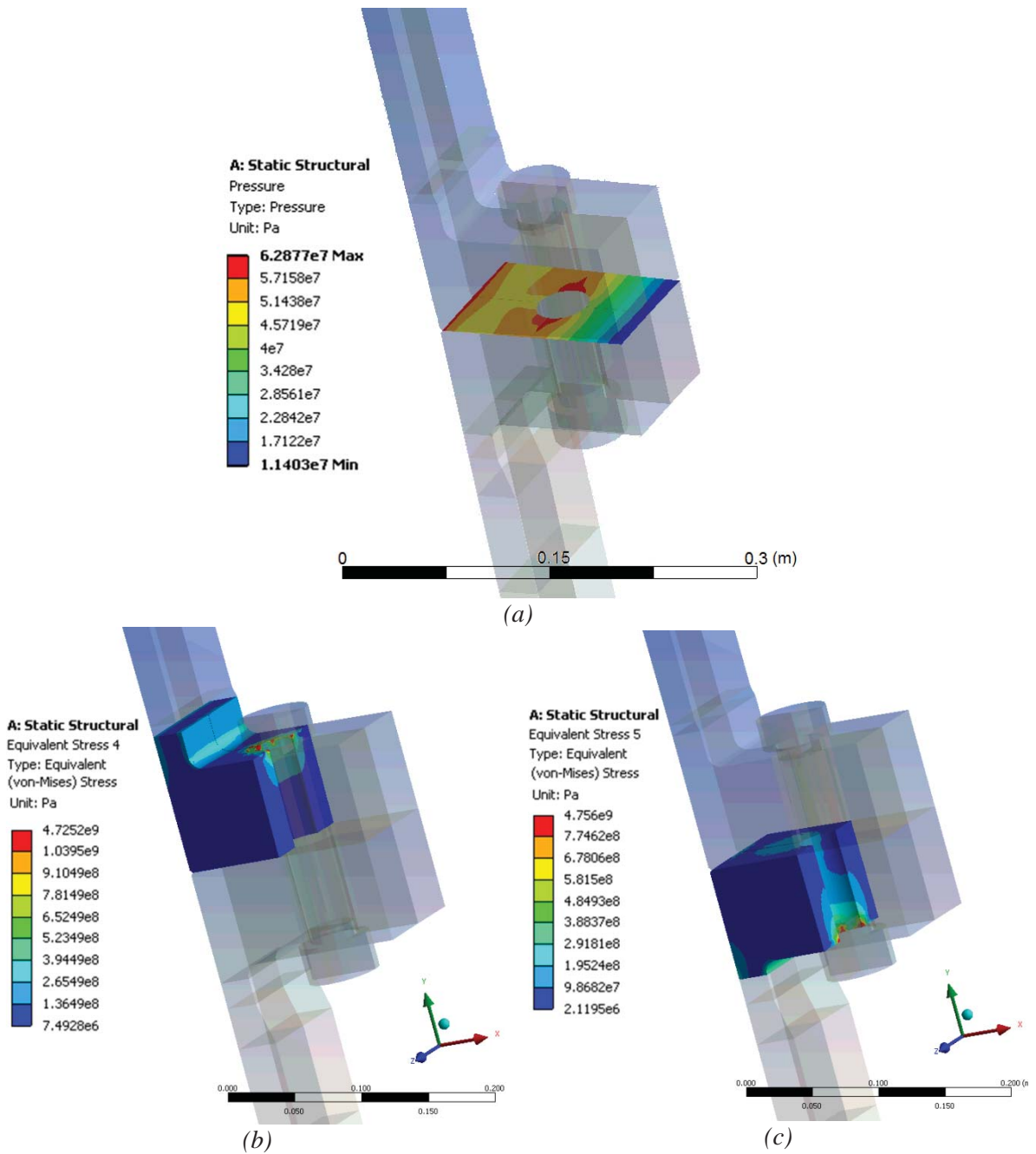
Fig. 15.   Results of the FE model and DOE analysis: a) Contact stress between upper and lower flanges (in Pa); b) Von Mises stress in upper flange (in Pa); c) Von Mises stress in lower flange (in Pa)
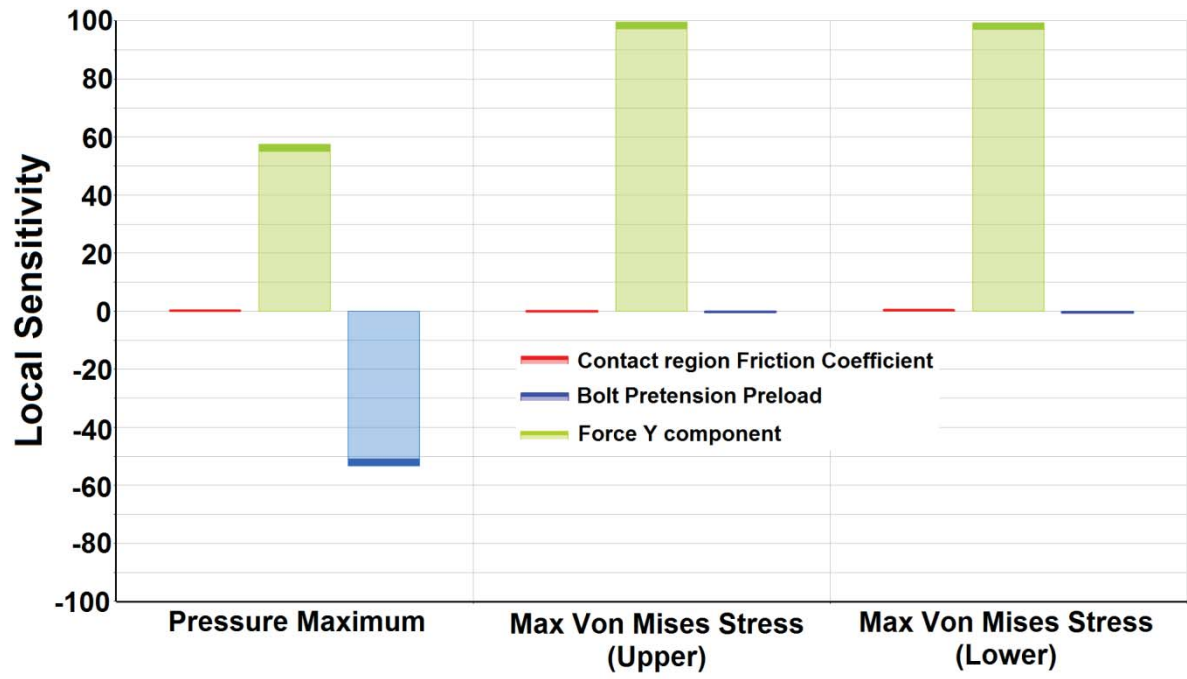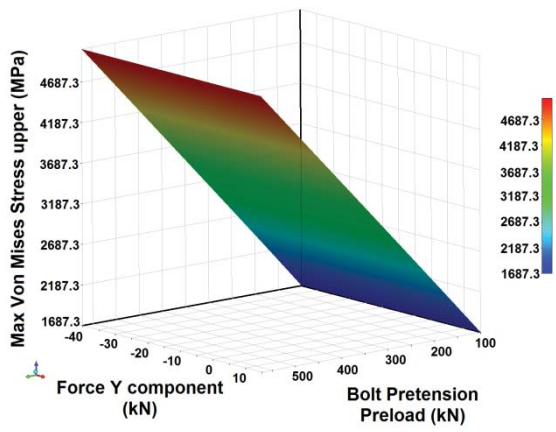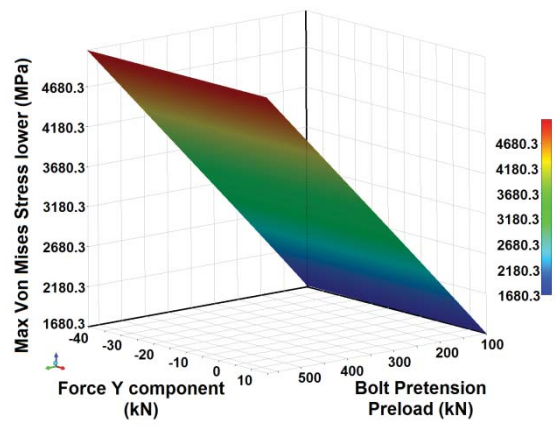
Fig. 16.   Sensitivity analysis

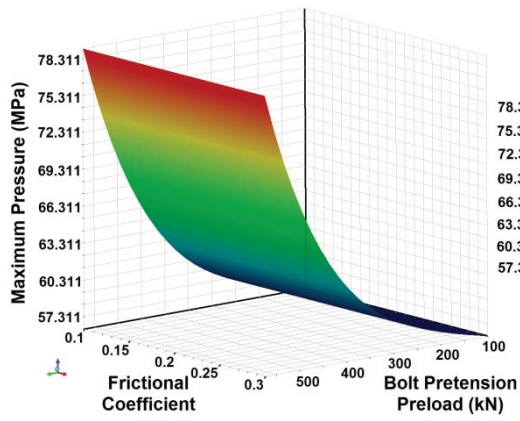*a)*   *b)*
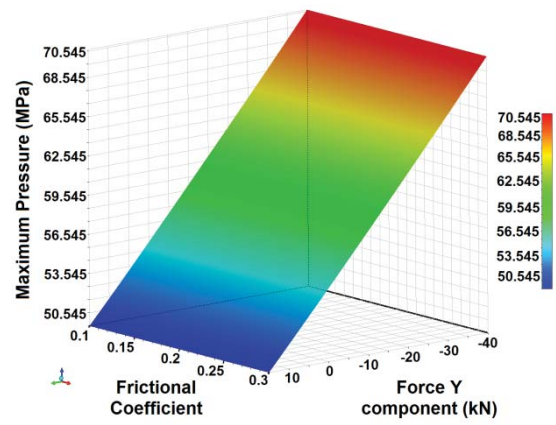
Fig. 17.   *DOE analysis: External part of the flange (upper and lower part. a) Bolt pretension vs Force Y in upper part of the flange; b) Bolt pretension vs Force Y in lower part of the flange*

Fig. 18. *DOE analysis: maximum pressure in contact between the flanges: a) Contact friction vs Bolt pretension; b) Contact friction vs Force Y.*

	Sy (MPa)	Su (MPa)	A (%)	Kv (+13ºC) (J)	Kv (-20ºC) (J)
Flange W (*)	422	557	24	62	13
Flange M (**)	383	536	28	---	10
S355 J2	>295	450-600	>18	---	>27

Table 1.   Experimental Results

(*) W: Working direction

(**) M: Manufacturing direction

Reference values obtained for S355J2 grade with 105 mm width from UNE-EN 10025-2 [24].

Yield strength (Sy), Tensile Strenght (Su), Deformation (A), Toughness (Kv)

Table 2.　　Wind turbine information

Wind power component	Values
Rotor diameter, D (m)	77
Swept area, A (m^2)	4 656.6
Nacelle weight, (kg)	50 000
Rotor + hub weight (kg)	31 000
Wind Speed, v (m/s)	5.21

Table 3.   Power and load on the wind turbine.

Loads	Values
Power (kW)	742.41
Avaliable Power (kW)	296.96
Wind force (kN)	46.57

Table 4. Stress values on the flange

Stress	
Max. Compression Stress $\sigma_{\max (c)}$ (MPa)	16.64
Max. Tensile Stress $\sigma_{\max (t)}$ (MPa)	9.38
Max. Compressive load (kN)	(-)32.57
Tensile Load (kN)	(+)18.37

Table 5. Values of parameters in the DOE

	Minimum Value	Initial Value	Maximum Value
Frictional Coefficient	0.1	0.1	0.3
Bolt preload (kN)	100	520	571
Force (Y axis) (kN)	-40	32.5	15

Table 6. Statistical parameters in the DOE analysis.

	P3 - Pressure Maximum	P4 - sint_b_ sup_ext Maximum	P5 - sint_b_ inf_ext Maximum	P6 - sint_b_ sup_tra nsition Maximum	P7 - sint_b_ inf_tra nsition Maximum	P8 - sint_b_ sup_int Maximum	P9 - sint_b_ inf_int Maximum	P10 - Stress Intensit y 2 Maximum
Coefficient of Determination (Best Value = 1)								
Learning Points	0.9945	0.9993	0.9990	0.9999	0.9997	0.9999	0.9999	0.9999
Relative Maximum Absolute Error (Best Value = 0%)								
Learning Points	19.1818	5.8119	8.4279	0.4350	3.2576	0.8412	1.7775	0.6130
Relative Average Absolute Error (Best Value = 0%)								
Learning Points	5.326735	1.9106	2.0452	0.1387	1.1117	0.3627	0.6299	0.2586

AUTHOR DECLARATION TEMPLATE

We wish to confirm that there are no known conflicts of interest associated with this publication and there has been no significant financial support for this work that could have influenced its outcome.

We confirm that the manuscript has been read and approved by all named authors and that there are no other persons who satisfied the criteria for authorship but are not listed. We further confirm that the order of authors listed in the manuscript has been approved by all of us.

We confirm that we have given due consideration to the protection of intellectual property associated with this work and that there are no impediments to publication, including the timing of publication, with respect to intellectual property. In so doing we confirm that we have followed the regulations of our institutions concerning intellectual property.

We understand that the Corresponding Author is the sole contact for the Editorial process (including Editorial Manager and direct communications with the office). He/she is responsible for communicating with the other authors about progress, submissions of revisions and final approval of proofs. We confirm that we have provided a current, correct email address which is accessible by the Corresponding Author and which has been configured to accept email from mar@constru.uniovi.es

Signed by all authors as follows:

Mar Alonso-Martínez, Gijon, Spain, May 2019
Jose Adam, Valencia, Spain, May 2019
Felipe Pedro Álvarez Rabanal, Gijon, Spain, May 2019
Juan José del Coz-Díaz , Gijon, Spain, May 2019